OAK RIDGE NATIONAL LABORATORY
operated by
UNION CARBIDE CORPORATION
NUCLEAR DIVISION
for the
U.S. ATOMIC ENERGY COMMISSION

ORNL - TM - 1966

COPY NO. - 52

DATE - September 12, 1967

THE VARIATION OF SHOCK OVERPRESSURE WITH DISTANCE IN AN EXPLOSIVELY DRIVEN SHOCK TUBE*

Lawrence Dresner
Civil Defense Research Project

*Research sponsored under Advanced Research Projects Agency Order No. 907

DISCLAIMER

PAGES 1 to 2

WERE INTENTIONALLY

LEFT BLANK

TABLE OF CONTENTS

THE VARIATION OF SHOCK OVERPRESSURE WITH DISTANCE IN AN EXPLOSIVELY DRIVEN SHOCK TUBE

Lawrence Dresner

1. INTRODUCTION

This is the third in a series of papers dealing with the propagation of shock waves in a tube. The first two papers (refs. 1 and 2) dealt with shock waves produced by detonating small amounts of high explosive in the tube. One of the aims of this previous work was to study the attenuation of shock waves by baffles, such as orifice plates, placed in the tubes.

The total energy (and thus the duration) of the shock waves produced by high explosives is limited by the largest yield that can be safely used. In the experiments reported in refs. 1 and 2, the largest yield used in the 4-in. shock tube at ORNL was about 5 grams of TNT.

The flexibility of the shock tube is increased if the total energy of the shock wave can be varied over a wide range, especially if it can be increased by as much as one to two orders of magnitude. To do this, high explosive has to be abandoned and other methods of driving the shock tube sought.

In this report, two new methods are studied theoretically and compared with the old method of using high explosive. In particular, the variation of shock overpressure with distance down the tube is calculated for the following three different ways of driving a shock tube:

1. Detonation of a small amount of high explosive in one end of the tube.

2. Rapid burning of smokeless powder in a closed volume (driver section) confined by a breakable membrane (G. Coulter, BRL, private communication to C. V. Chester, ORNL). When the smokeless powder burns, it heats

the air causing its pressure to increase. The amount of smokeless powder is chosen so that when it is all burned the pressure of the air in the driver section is the pressure at which the membrane ruptures. After rupture, the hot gas in the driver section rushes down the tube driving a shock wave before it.

3. Detonation of an explosive gas mixture confined by a breakable membrane.

Far enough down the tube the three variations of shock overpressure with distance become indistinguishable if the total energy is the same in all three methods. However, near the driver end of the tube, the three are different. The shock overpressures produced in methods 2 and 3 above vary in rather unusual ways with distance down the tube (see Figs. 2 and 3). This unusual behavior is analyzed in detail and shown to be due to the propagation of rarefaction waves through the gas behind the shock front.

Section 2 gives the results in the form of plots of peak overpressure vs distance down the tube. Section 3 contains a discussion based on the method of characteristics of method 2 of driving a shock tube. Section 4 contains a similar discussion of method 3. Since the information derived in these analytic discussions is incomplete, numerical calculations were undertaken to round out our understanding of the flow processes in these two methods. These numerical calculations are discussed in detail in Section 5.

2. RESULTS

The shock overpressure produced by detonation of a small amount of high explosive in a tube has already been discussed in other reports of the author's.[1,2] There the solution was given to the following idealized problem: A plane sheet of explosive is detonated at time $t = 0$ in the plane $X = 0$ in an infinite, homogeneous atmosphere (pressure = p_o, density = ρ_o), instantaneously depositing there an energy $2E$ per unit area. What is the shock overpressure Δp when the shock fronts have reached the planes $\pm X$? The answer to this problem is shown in Fig. 1, where $\Delta p/p_o$ is plotted against $p_o X/E$. The curve was calculated numerically by the method of von Neumann and Richtmyer.[3] The high- and low-overpressure asymptotes are

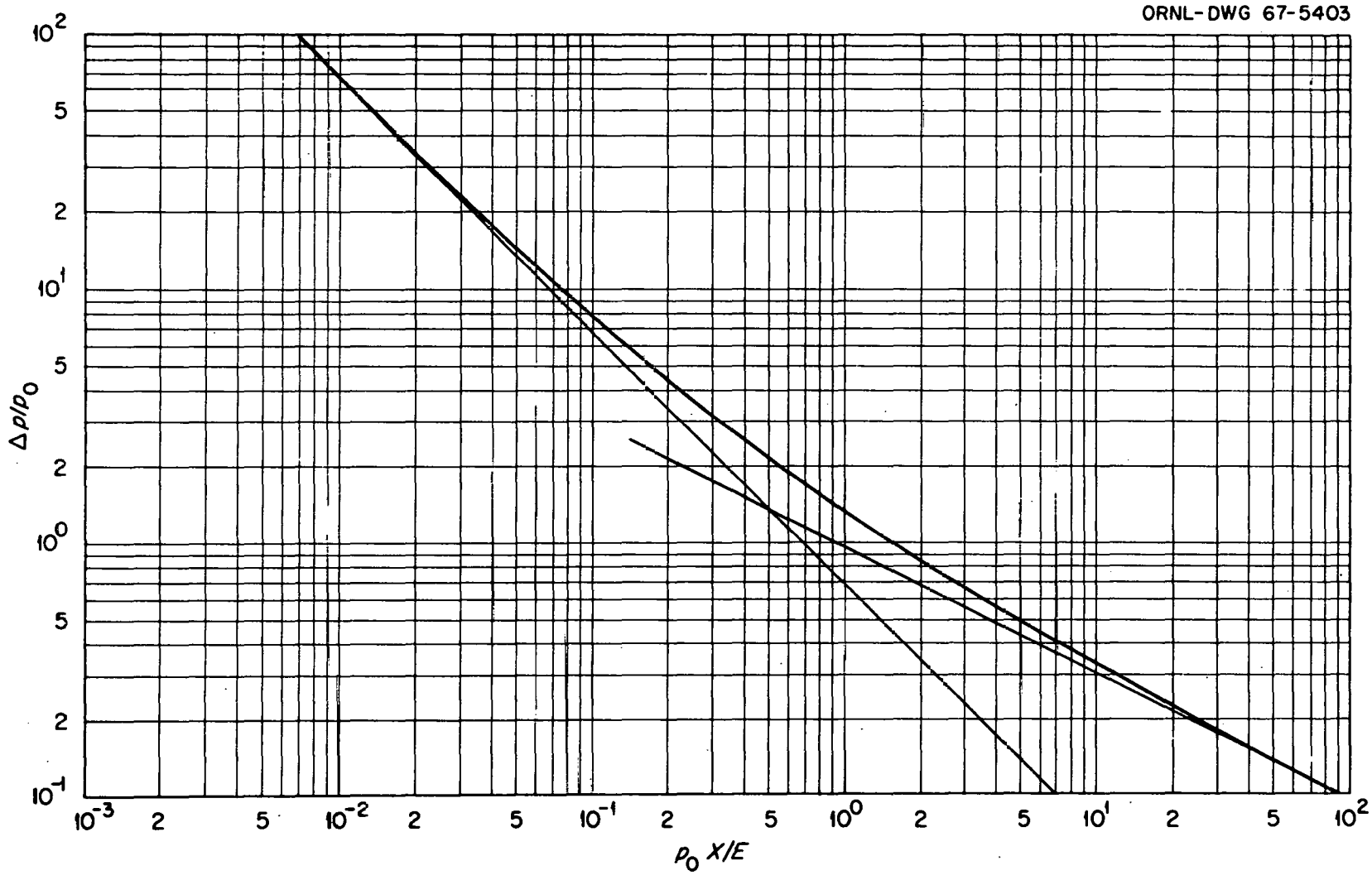

Fig. 1. $\Delta p/p_0$ vs p_0X/E Explosion in an Infinite, Homogeneous Atmosphere. Δp is the shock overpressure, p_0 is the initial pressure of the atmosphere, X is the distance from the plane of the explosion, and 2E is the energy per unit area of the explosion.

$$\frac{\Delta p}{p_0} = 0.6875 \frac{E}{p_0 X} \quad , \tag{1a}$$

and

$$\frac{\Delta p}{p_0} = 0.9661 \left(\frac{E}{p_0 X}\right)^{1/2} , \tag{1b}$$

respectively for a perfect gas with a ratio γ of specific heats equal to 1.4.

In the actual explosion of a small amount of high explosive in the end of a tube, several additional phenomena occur. In the first place, not all of the energy of the explosive finds its way into air blast. Some of it is transferred to the pipe wall as heat by the hot bubble of gas created by the explosion. Secondly, the air blast does not assume the form of a plane blast wave until it has progressed a short distance down the tube. Thirdly, friction with the pipe walls causes some attenuation in the shock overpressure. The first and third phenomena are dealt with in references 1 and 2. For distances not greater than about 50 diameters in ordinary iron pipe, Fig. 1 (with a yield corrected for heat loss to the wall) gives the variation of shock overpressure with distance down the tube correctly.

We shall assume in method (2) that the gas in the driver section is heated uniformly. If an amount of heat q is released per gram of gas in the driver section, the pressure of the gas at the instant of membrane rupture is greater than its original pressure p_0 by an amount p_* given by

$$\frac{p_*}{(\gamma - 1)\, \rho_0} = q \quad . \tag{2}$$

We shall assume henceforth that $p_* \gg p_0$.

If we fix $\gamma = 1.4$ once and for all, the entire problem may be specified by the physical variables p_*, p_0, ρ_0, and L, the length of the driver section. Since $p_* \gg p_0$, we may drop p_0 from the list. Dimensional

analysis then indicates that the variation of shock overpressure with distance X down the tube must have the form

$$\frac{\Delta p}{p_*} = f\left(\frac{X}{L}\right) , \qquad (3)$$

where f is an as yet undetermined function.

When $X \gg L$, Eq. (3) should go over into Eq. (1a). Since $E = \rho_0 qL$, this means that

$$f\left(\frac{X}{L}\right) \sim \frac{1.719}{X/L} \qquad (X \gg L,\ \gamma = 1.4) . \qquad (4)$$

When the membrane first ruptures, the situation is the same as that in a conventional gas-driven shock tube. A shock front and a contact surface propagate forward in the tube while a rarefaction propagates backwards. The shock overpressure remains constant at least until this rarefaction reflects off the end of the tube and catches up with the shock front. In the next section it is shown that the rarefaction catches up with the shock front when $X/L = 3.817$; for smaller values of X, $\Delta p/p_*$ may be calculated with the Taub equation,[4] according to which

$$f\left(\frac{X}{L}\right) = 0.4609 \qquad (1 \le X \le 3.817,\ \gamma = 1.4) \qquad (5)$$

Equations (4) and (5), which give the behavior of f(X/L) for large and small X/L, respectively, are plotted in Fig. 2 as thin lines. Plotted as a thick line is a curve calculated numerically by the method of von Neumann and Richtmyer.[3] It appears that f(X/L) is very close to the value given by Eq. (5) for $X/L \le 3.729$ [the value of X/L at which Eqs. (4) and (5) intersect] and very close to the value given by Eq. (4) for $X/L \ge 3.729$.

In method (3), the gas in the driver section is not uniformly heated. Instead a detonation is initiated at X = 0 and allowed to propagate through the explosive gas mixture in the driver section. When the detonation front reaches the membrane, the latter ruptures and the burned gas escapes, driving a shock wave before it.

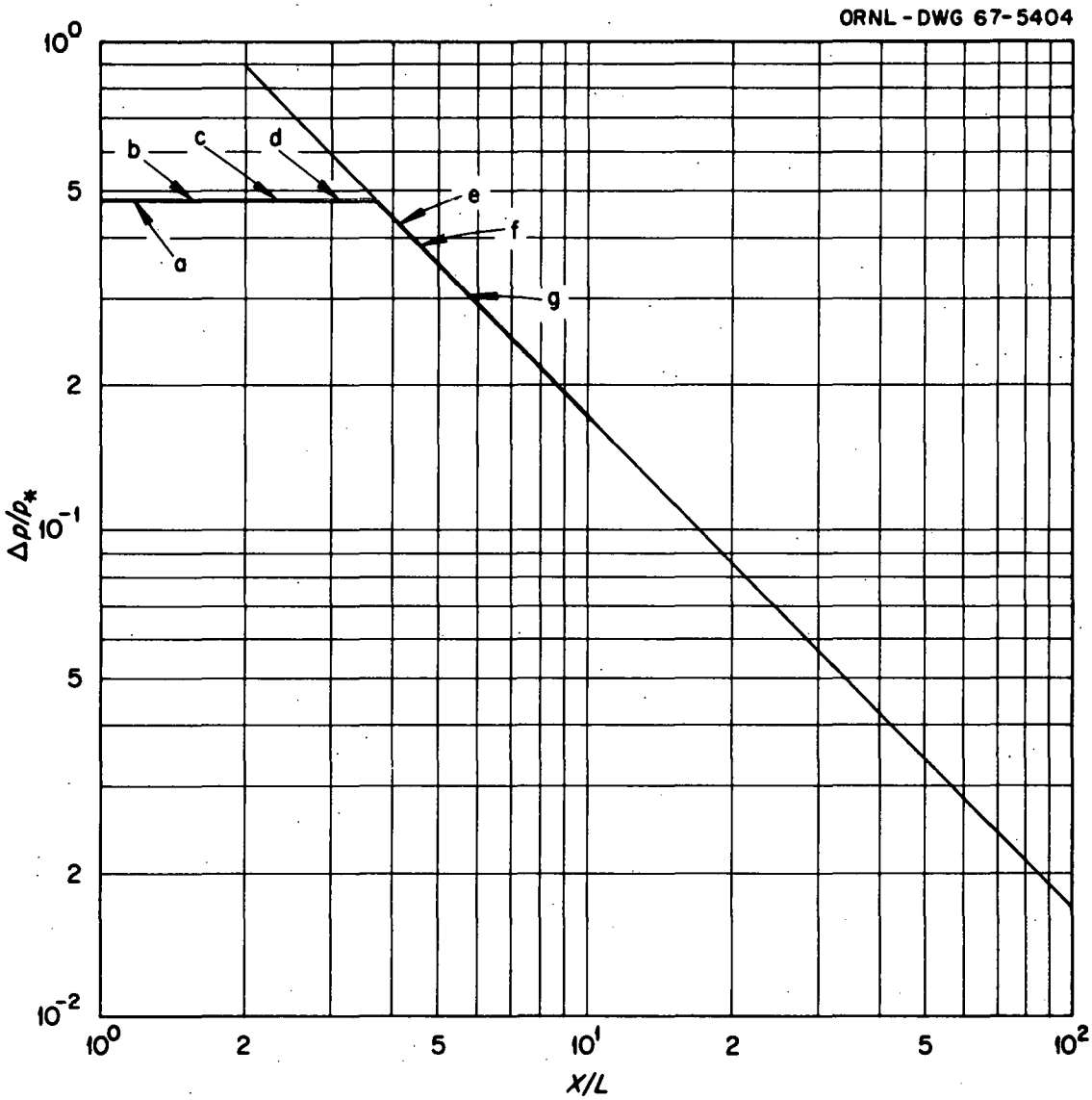

Fig. 2. The Function $f(X/L) = \Delta p/p_*$ vs X/L. p_* is the initial overpressure in the driver section, L is the length of the driver section, Δp is the shock overpressure, and X is the position of the shock front measured from the driver end of the tube.

q and p_* are defined as in case (2), i.e., q is the heat released by chemical reaction per gram of explosive gas mixture, and p_* is the uniform rise in pressure the burned gas would experience if it were confined indefinitely in its original volume. γ is taken to be the same for the burned gas as for the unburned explosive mixture. By the same dimensional argument as before it follows that

$$\frac{\Delta p}{p_*} = g\left(\frac{X}{L}\right), \tag{6}$$

where g is an as yet undetermined function. When $X \gg L$, Eq. (6) also goes over into Eq. (1a), i.e.,

$$g\left(\frac{X}{L}\right) \sim \frac{1.719}{X/L} \qquad (X \gg L,\ \gamma = 1.4) \tag{7}$$

When X/L is small, however, g behaves very differently from f. In the first place, until the detonation front reaches the end of the explosive gas mixture, $\Delta p/p_*$ remains constant. If the detonation is a Chapman-Jouguet detonation, this constant is 2 when $p_* \gg p_0$, as shown in section four of this report. Thus,

$$g\left(\frac{X}{L}\right) = 2 \qquad (X < L)\ . \tag{8}$$

When the detonation front reaches the end of the explosive gas mixture, it changes abruptly into an ordinary shock front. The shock overpressure drops discontinuously to $1.56\ p_*$ at X = L, as is also shown in section four.

Equations (7) and (8), which give the behavior of g(X/L) for large and small X, respectively, are plotted in Fig. 3 as thin lines. Shown as a thick line is a curve calculated numerically by the method of von Neumann and Richtmyer. One can see that g(X/L) has a most unusual behavior, which is discussed further in section five.

3. UNIFORM HEATING

Figure 4 shows a wave diagram describing the flow in method (2) after the membrane ruptures. The line Ot is the time axis; the line

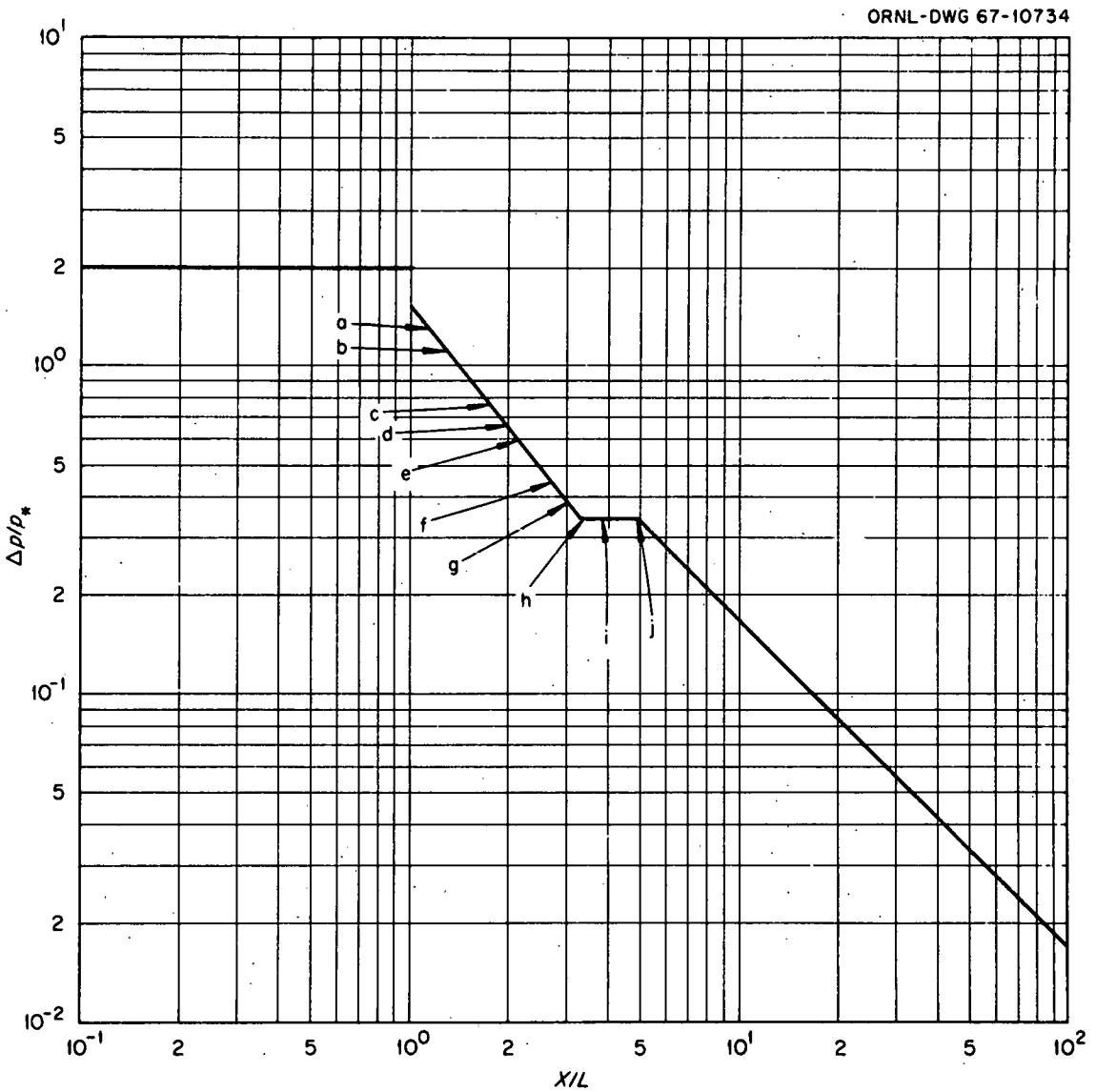

Fig. 3. The Function $g(X/L) = \Delta p/p_*$ vs X/L. p_* is the uniform rise in pressure the burned gas would experience if confined indefinitely in its original volume, Δp is the overpressure at the shock (or detonation) front, L is the length of the driver section, and X is the position of the shock (or detonation) front measured from the driver end of the tube.

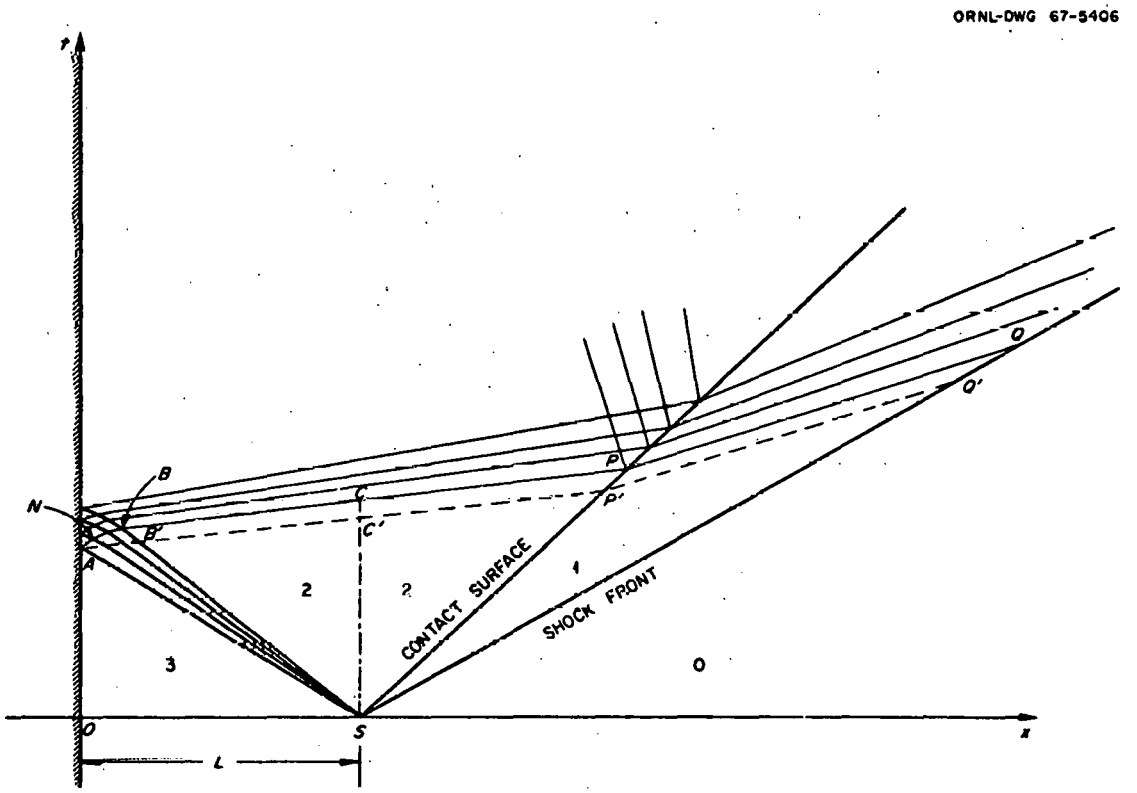

Fig. 4. Wave Diagram for the Case of Uniform Heating (Method 2).

Ox is the space axis. The line x = 0 represents the end of the tube. Point S marks the position of the membrane before it ruptures. SQ is the shock front and SP the contact surface between the hot gas that was originally behind the membrane and the shocked gas that was originally in front of it. A rarefaction wave is shown propagating backwards from S, reflecting from the end of the tube, crossing the contact surface and eventually catching up with the shock front.

The shock front, contact surface, and rarefaction wave separate four regions of uniform flow labeled 0, 1, 2, and 3 in the wave diagram. Each region is described by two thermodynamic state variables and a flow velocity u. Actually, four different thermodynamic variables are in common use, namely, the pressure p, the density ρ, the speed of sound c, and the specific volume τ. These four are connected by two relations, viz.,

$$\gamma p = \rho c^2 , \tag{9a}$$

$$\rho\tau = 1 , \tag{9b}$$

so that only two are independent.

Region 0 is the region of as yet undisturbed air. Its pressure is p_0, its density ρ_0, its flow velocity $u_0 = 0$. Region 3 is the region of still stationary driver air. Therefore

$$p_3 = p_* , \tag{10a}$$

$$\rho_3 = \rho_0 , \tag{10b}$$

$$c_3 = \sqrt{\gamma\, p_*\, \tau_0} , \tag{10c}$$

$$u_3 = 0 . \tag{10d}$$

Region 2 is the region of expanded driver air. Its state is connected with the state in region 3 by the adiabatic law

$$p_3^{(1-\gamma)/2\gamma} c_3 = p_2^{(1-\gamma)/2\gamma} c_2 , \tag{11a}$$

and by the constancy of one of the Riemann invariants

$$\frac{2c_3}{\gamma - 1} + u_3 = \frac{2c_2}{\gamma - 1} + u_2 \ . \tag{11b}$$

Region 1 is the region of shocked air. Its state is related to the state 0 by the Rankine-Hugoniot equations. Since, by hypothesis, $p_* \gg p_0$, we can use the limiting form these equations take for strong shocks, viz.,

$$\frac{\rho_0}{\rho_1} = \mu^2 \equiv \frac{\gamma - 1}{\gamma + 1} \ , \tag{12a}$$

$$\rho_0 u_1 U - p_1 \ , \tag{12b}$$

$$\rho_0 u_1^2 = p_1 (1 - \mu^2) \ , \tag{12c}$$

where U is the shock veloqity. Finally, since regions 1 and 2 are separated by a contact surface,

$$p_2 = p_1 \ , \tag{13a}$$

$$u_2 = u_1 \ . \tag{13b}$$

Using Eqs. (10-13), we can solve for the ratio p_1/p_* as follows:

$$\sqrt{p_1 \tau_0 (1 - \mu^2)} = u_1 \ , \qquad [12c] \tag{14a}$$

$$= u_2 \ , \qquad [13b] \tag{14b}$$

$$= \frac{2c_3}{\gamma - 1}\left(1 - \frac{c_0}{c_3}\right) \ , \qquad [11b] \tag{14c}$$

$$= \frac{2}{\gamma - 1}\sqrt{\gamma p_3 \tau_0}\left(1 - \frac{c_2}{c_3}\right) \ , \qquad [9a] \tag{14d}$$

$$= \frac{2}{\gamma - 1}\sqrt{\gamma p_3 \tau_0}\left[1 - \left(\frac{p_2}{p_3}\right)^{(\gamma-1)/2\gamma}\right] \ , \qquad [11a] \tag{14e}$$

$$= \frac{2}{\gamma - 1}\sqrt{\gamma p_3 \tau_0}\left[1 - \left(\frac{p_1}{p_3}\right)^{(\gamma-1)/2\gamma}\right] \ , \qquad [13a] \tag{14f}$$

$$= \frac{2}{\gamma - 1}\sqrt{\gamma p_* \tau_0}\left[1 - \left(\frac{p_1}{p_*}\right)^{(\gamma-1)/2\gamma}\right] \ . \qquad [10a] \tag{14g}$$

Here the numbers in brackets denote the equation used in obtaining the equality written on the same line. The last equality may be written

$$\frac{p_1}{p_*} = \frac{2\gamma\,(\gamma+1)}{(\gamma-1)^2}\left[1 - \left(\frac{p_1}{p_*}\right)^{(\gamma-1)/2\gamma}\right]^2 . \qquad (15)$$

When $\gamma = 1.4$, Eq. (15) may be solved by trial and error to give

$$\frac{p_1}{p_*} = 0.4609 \qquad (\gamma = 1.4) . \qquad (16)$$

Equations (10-13) may now be used to find the remaining unknowns. The results are given in the following table.

Table 1. State Variables for $\gamma = 1.4$

Region i	0	1	2	3
p_i/p_*	$\ll 1.000$	0.4609	0.4609	1.000
ρ_i/ρ_0	1.000	6.000	0.5751	1.000
c_i/U	$\ll 1.000$	0.4410	1.424	1.591
u_i/U	0	0.8333	0.8333	0

Using the figures in Table 1, we can calculate the abscissa X_0 of the point Q at which the reflected rarefaction first overtakes the shock wave SQ. However, instead of proceeding directly with that calculation we first obtain a lower limit for X_0. As shown in the wave diagram, the portion AB of the leading characteristic of the reflected rarefaction is curved and in fact is concave downwards. (We shall subsequently prove that this is so.) The portions BP and PQ on the other hand are straight lines since they have constant slopes dx/dt equal to $u_2 + c_2$ and $u_1 + c_1$, respectively. Let us now extend a line through A parallel to BP (line AB'P') which intersects the path of the contact surface SP in P'. Through P' we extend a line P'Q' parallel to PQ which intersects the path SQ of the shock in Q'. Since AB is concave downwards, the abscissa X_0 of Q is greater than the abscissa X_0' of Q! We can determine the value of X_0' by writing in terms of X_0'

and X_2' (the abscissa of P') and the velocities u_i, c_i, and U the following two requirements, namely: (1) the projection on the time axis of SQ' is the sum of the projections on the time axis of SA, AP', and P'Q'; and (2) the projection on the time axis of SP' is the sum of the projections on the time axis of SA and AP'. The slopes dx/dt of SA, AP', P'Q', SP', and SQ' are, respectively, $u_3 - c_3$, $u_2 + c_2$, $u_1 + c_1$, u_1, and U. Thus

$$\frac{X_0' - L}{U} = \frac{L}{-u_3 + c_3} + \frac{X_2'}{u_2 + c_2} + \frac{X_0' - X_2'}{u_1 + c_1} \tag{17a}$$

$$\frac{X_2' - L}{u_1} = \frac{L}{-u_3 + c_3} + \frac{X_2'}{u_2 + c_2} \tag{17b}$$

It follows from these equations and the state variables given in Table 1 that

$$\frac{X_0'}{L} = 3.730 , \tag{18a}$$

$$\frac{X_2'}{L} = 2.415 . \tag{18b}$$

Thus Eq. (16) must hold at least until the shock front reaches an abscissa $X_0' = 3.730L$.

To show that this value is actually a lower limit to X_0, i.e., to show that $X_0 > X_0'$, it is enough to show that the arc AB is concave downwards. This we do as follows. Owing to the constancy of a Riemann invariant along AB we may write

$$\frac{2c_3}{\gamma - 1} = u + \frac{2c}{\gamma - 1} = \frac{1}{2}\left[\frac{\gamma + 1}{\gamma - 1}(u + c) + \frac{\gamma - 3}{\gamma - 1}(u - c)\right] , \tag{19}$$

where u and c are the flow velocity and speed of sound at any point N along AB. The second equality is simply an identity. Now let s represent the arc length along AB measured positively from A. Then from (19) we get

$$\frac{d}{ds}(u + c) = \frac{3 - \gamma}{\gamma + 1}\frac{d}{ds}(u - c) . \tag{20}$$

Now $dx/dt = u - c$ along the line SN. Thus

$$\frac{d}{ds}(u - c) > 0 , \tag{21}$$

since, for example, $u - c$ is more negative along SA than SN, etc. Hence, if $\gamma \leq 3$,

$$\frac{d}{ds}(u + c) \geq 0 , \tag{22}$$

which says that dx/dt increases along AB with increasing arc length s from A. This means, however, that AB is concave downwards.

Now let us calculate exactly the value of X_o. We begin by erecting a perpendicular at S that intersects the lines A'P' and BP in the points C' and C, respectively. Since the pairs of triangles SCP and SC'P' and SPQ and S'P'Q' are respectively similar,

$$\frac{X_o' - L}{X_o - L} = \frac{SQ'}{SQ} = \frac{SP'}{SP} = \frac{SC'}{SC} . \tag{23}$$

In order to calculate the ratio SC'/SC we need to find the equation of the arc AB. The differential equation of AB is

$$\frac{dx}{dt} = u + c = \frac{4c_3}{\gamma + 1} + \frac{3 - \gamma}{\gamma + 1}(u - c) . \tag{24}$$

The second equality follows by use of Eq. (19). If (x,t) are the coordinates of N,

$$u - c = \frac{x - L}{t} , \tag{25}$$

since the slope dx/dt of SN is $u - c$. Thus the differential equation of AB becomes

$$\frac{dx}{dt} = \frac{4c_3}{\gamma + 1} + \frac{3 - \gamma}{\gamma + 1}\left(\frac{x - L}{t}\right) . \tag{26}$$

If we introduce the variables

$$\xi = \frac{x - L}{c_3 t} , \tag{27a}$$

$$\tau = \frac{c_3 t}{L} , \tag{27b}$$

(26) becomes

$$\tau \frac{d\xi}{d\tau} + 2\left(\frac{\gamma - 1}{\gamma + 1}\right) \xi = \frac{4}{\gamma + 1} . \tag{28}$$

When $\tau = 1$, i.e., when $t = L/c_3$, $x = 0$, i.e., $\xi = -1$. Equation (28) can be solved by separation of variables and yields

$$\tau = \left(\frac{2}{\gamma + 1} \cdot \frac{\gamma - 1}{\gamma + 1} \xi\right)^{-[(\gamma+1)/2(\gamma-1)]} \tag{29}$$

We shall need the intersection B of this curve with the trailing characteristic SB of the rarefaction, i.e., with the line

$$\frac{x - L}{t} = u_2 - c_2 , \tag{30a}$$

or

$$\xi = \frac{u_2 - c_2}{c_3} = -0.3715 . \tag{30b}$$

Here we have used the state variables given in Table 1. Substituting (30b) into (29), we find $\tau = 1.394$. Thus the coordinates of B are

$$X_B = 0.4823\ L , \tag{31a}$$

$$t_B = 1.394 \frac{L}{c_3} . \tag{31b}$$

The equation of the line BC is

$$(x - x_B) = (u_2 + c_2)(t - t_B) . \tag{32}$$

It follows from (32), (31), and Table 1 that when $x = L$,

$$t = 1.759 \frac{L}{c_3} = SC . \tag{33}$$

The equation of the line AB'C' is

$$X = (u_2 + c_2)(t - \frac{L}{c_3}) . \tag{34}$$

It follows from (34) and Table 1 that when $x = L$

$$t = 1.705 \frac{L}{c_3} = SC' . \tag{35}$$

Finally, from (33), (35), (23), and (18a), it follows that

$$\frac{X_o}{L} = 3.817 . \tag{36}$$

4. DETONATION OF AN EXPLOSIVE GAS MIXTURE

Until the detonation front reaches the end of the driver section, the wave diagram (Fig. 5) is that of a Chapman-Jouguet detonation followed by a rarefaction wave.[5] Because the flow behind a Chapman-Jouguet detonation is sonic relative to the front, the leading edge of the rarefaction coincides with the detonation front. Behind the rarefaction is a region of stationary burned gas of uniform pressure and density.

When the detonation front reaches the end of the driver section (point P), conditions change abruptly, combustion energy no longer being supplied to the gas. The burned gas in the region $x < L$ now acts as a driver gas, while the air in the region $x > L$ acts as the gas being driven. A shock, contact surface, and rarefaction wave emanate from point P exactly as they do from point S in Fig. 4. They are shown schematically in Fig. 5. The contact surface separates the air that has passed through the shock front from the burned gas that has expanded through the rarefaction. Because of the presence of the rarefaction emanating from the origin O, the trajectories of the shock front and the contact surface cannot be calculated as simply as they were in the last section. However, in the neighborhood of the point P, the methods of the last section apply mutatis mutandis, and we shall be able at least to calculate the initial overpressure behind the shock front at P.

Let us begin by calculating the condition of the gas at position 1 just behind the Chapman-Jouguet detonation front. Fig. 6 shows the

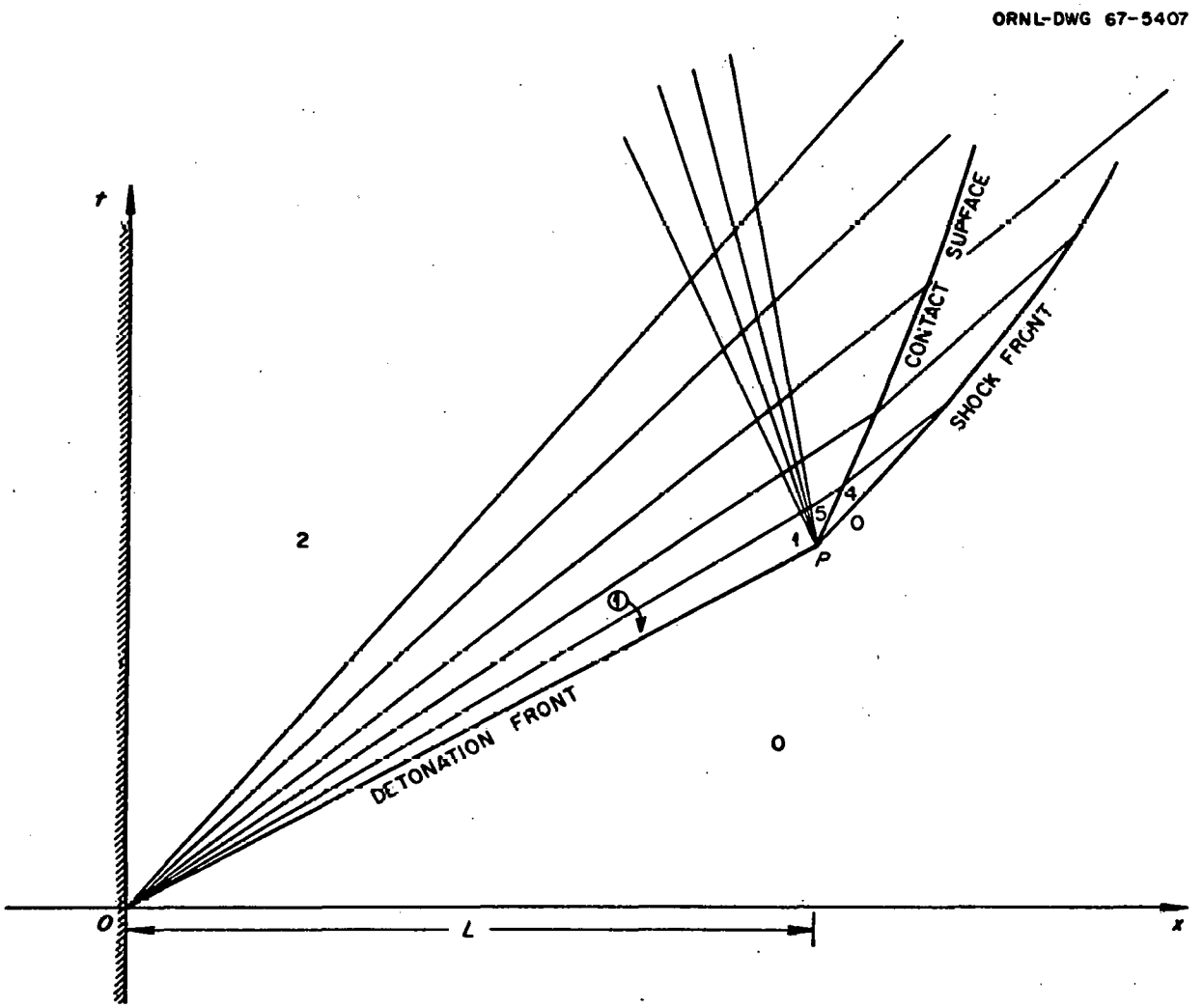

Fig. 5. Wave Diagram for the Case of an Exploding Gas Mixture (Method 3).

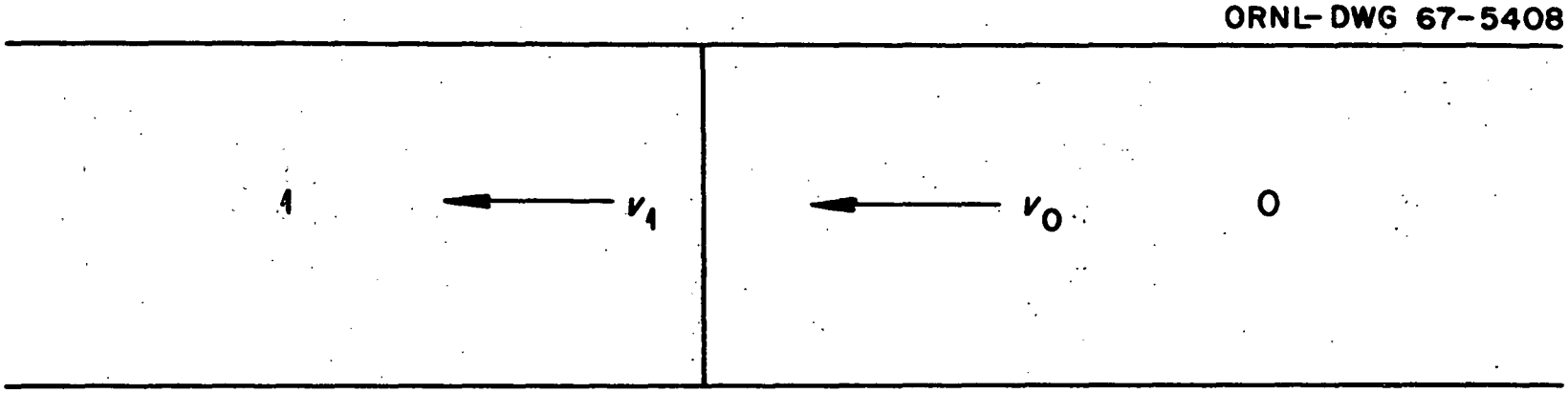

Fig. 6. Schematic Diagram of the Flow Through a Chapman-Jouguet Detonation Front in a System of Reference Stationary with Respect to the Front.

flow conditions in a frame of reference at rest with respect to the detonation front. v_0 and v_1, the flow velocities of the gas on the two sides of the detonation front in this frame of reference, are measured positively in the direction of the arrows. Since u_0, the velocity of the unburned gas in the laboratory frame of reference, is zero,

$$U = v_0 , \tag{37a}$$

$$u_1 = U - v_1 = v_0 - v_1 , \tag{37b}$$

where U is the velocity of the detonation front, and u_1 is the flow velocity of the burned gas in the laboratory frame of reference, and both are measured positively to the right.

If we now let m be the mass flux density (g $cm^{-2}sec^{-1}$) of gas through the front, we see that

$$\rho_0 v_0 = \rho_1 v_1 = m . \tag{38a}$$

Now we consider the change in momentum of the slug of fluid passing through the detonation front in one second. It is given by

$$mv_1 - mv_0 = p_0 - p_1 . \tag{38b}$$

The change in energy of the same slug of fluid is given by

$$\frac{1}{2} mv_1^2 + mc_1 - \frac{1}{2} mv_0^2 - me_0 = p_0 v_0 - p_1 v_1 , \tag{38c}$$

where e_i is the internal energy of the gas in region i per unit mass plus the energy q_i that could be released per unit mass by chemical reaction. Thus q_i is the potential energy of chemical reaction per unit mass of gas in region i. By hypothesis

$$q_1 = 0 , \tag{38d}$$

$$q_0 = \frac{p_*}{\rho_0(\gamma - 1)} . \tag{38e}$$

Equation (38e) defines p_*. Thus

$$e_0 = \frac{p_0 \tau_0}{\gamma - 1} + \frac{p_* \tau_0}{\gamma - 1} \quad , \tag{39a}$$

$$e_1 = \frac{p_1 \tau_1}{\gamma - 1} \quad . \tag{39b}$$

If we eliminate v_0, v_1, and m from Eqs. (38) and use Eqs. (39), we can express τ_1 in terms of p_1 as follows:

$$\frac{\tau_1}{\tau_0} = \frac{p_0 + \mu^2 p_1 + (1 - \mu^2)\, p_*}{p_1 + \mu^3 p_0} \quad . \tag{40}$$

According to the Chapman-Jouguet hypothesis, the condition

$$\frac{d\tau_1}{dp_1} = \frac{\tau_1 - \tau_0}{p_1 - p_0} \quad , \tag{41}$$

holds for an actual detonation. If we calculate $d\tau_1/dp_1$ from (40) and eliminate τ_1 between (40) and (41), we get

$$\Delta p = p_* + \Delta p \, \frac{p_* + (1 + \mu^2)\, p_0}{\Delta p + (1 + \mu^2)\, p_0} \quad , \tag{42a}$$

$$\Delta p \equiv p_1 - p_0 \quad . \tag{42b}$$

In the limiting case in which $p_* \gg p_0$, (42a) simplified to

$$p_1 = \Delta p = 2p_* \qquad (p_* \gg p_0) \quad . \tag{42c}$$

From (40) it then follows that

$$\frac{\tau_1}{\tau_0} = \frac{1 + \mu^2}{2} \qquad (p_* \gg p_0) \quad . \tag{43}$$

If we now substitute $\rho_0 v_0$ for m in (38b) and use (37a,b), we find

$$\rho_0 \, U \, u_1 = \Delta p \quad . \tag{44a}$$

Using (37b) and (38a), we can write

$$u_1 = m \, (\tau_0 - \tau_1) \quad . \tag{44b}$$

Using (44b) to eliminate m in (38b) and using (43), we get

$$\rho_0 u_1^2 = \Delta p \frac{1 - \mu^2}{2} \quad . \tag{44c}$$

From (44c) and (44a), it follows that

$$\frac{u_1}{U} = \frac{1 - \mu^2}{2} \quad . \tag{45a}$$

From (45a), (44c), (42c), (43), and (9a), it follows that

$$\frac{c_1}{U} = \frac{1 + \mu^2}{2} \quad . \tag{45b}$$

Thus

$$u_1 + c_1 = U \quad . \tag{45c}$$

as required by a theorem of Jouguet's. Finally, using (44a), (45a), and (9a), we get

$$\frac{U}{c_0} = \sqrt{\frac{4}{1 + \mu^2} \frac{p_*}{p_0}} \quad . \tag{45d}$$

The state variables p, τ, c, and u at any point in the rarefaction wave behind the detonation front can be determined from the relations

$$u + c = \frac{x}{t} \quad , \tag{46a}$$

$$\frac{2c}{\gamma - 1} - u = \frac{2c_1}{\gamma - 1} - u_1 \quad , \tag{46b}$$

$$\frac{p}{p_1} = \left(\frac{c}{c_1}\right)^{2\gamma/(\gamma-1)} \quad ; \quad \frac{\tau}{\tau_1} = \left(\frac{c}{c_1}\right)^{-2/(\gamma-1)} \quad . \tag{46c}$$

Equation (46a) gives two equivalent expressions for the slope dx/dt of the straight-line characteristics of the rarefaction wave emanating from O, Eq. (46b) expresses the constancy of a Riemann invariant along the cross characteristics, and Eqs. (46c) are two equivalent forms of the adiabatic law.

Using Eqs. (46a), (46b), (45a), and (45b), we find

$$\frac{c}{U} = \frac{1 - \mu^2}{2} + \mu^2\left(\frac{x}{Ut}\right) , \tag{47a}$$

$$\frac{c}{c_1} = \frac{1 - \mu^2}{1 + \mu^2} + \frac{2\mu^2}{1 + \mu^2}\left(\frac{x}{Ut}\right) , \tag{47b}$$

$$\frac{u}{U} = (1 - \mu^2)\left(\frac{x}{Ut}\right) - \frac{1 - \mu^2}{2} . \tag{47c}$$

Using (47b) and (46c), we can find p and τ.

X = Ut is the distance traveled by the detonation front in time t. From Eqs. (47) it is clear that the pressure, density, and velocity profiles behind the detonation front depend only on the ratio x/X. When x/X = 1/2, u = 0. For x/X < 1/2, all the state variables are constant and have the value they have for x/X = 1/2. This then determines the state variables in region 2 in Fig. 5. The pressure, density, sonic velocity, and flow velocity profiles behind the detonation front are plotted in Fig. 7 for $\gamma = 1.4$. It is these profiles which are used as the initial conditions in the numerical calculations mentioned in connection with Fig. 3.

By a repetition of the argument leading to Eq. (15) we can calculate the pressure just behind the shock front in the immediate vicinity of P. However, now the driver gas has the state variables p_1, τ_1, u_1 given by Eqs. (42c), (43), (45a), and (45d). The equation analogous to Eq. (15) is now

$$\left(\frac{p_4}{2p_*}\right)^{(\gamma - 1)/2\gamma} + \frac{\gamma - 1}{2\gamma}\sqrt{2}\left(\frac{p_4}{2p_*}\right)^{1/2} = 1 + \frac{\gamma - 1}{2\gamma} , \tag{48}$$

which has the solution

$$\frac{p_4}{p_*} = 1.556 , \tag{49}$$

for $\gamma = 1.4$. This means that when the detonation front reaches the end of the driver section and is replaced abruptly by a shock the shock overpressure jumps discontinuously from $2p_*$ to $1.556\ p_*$.

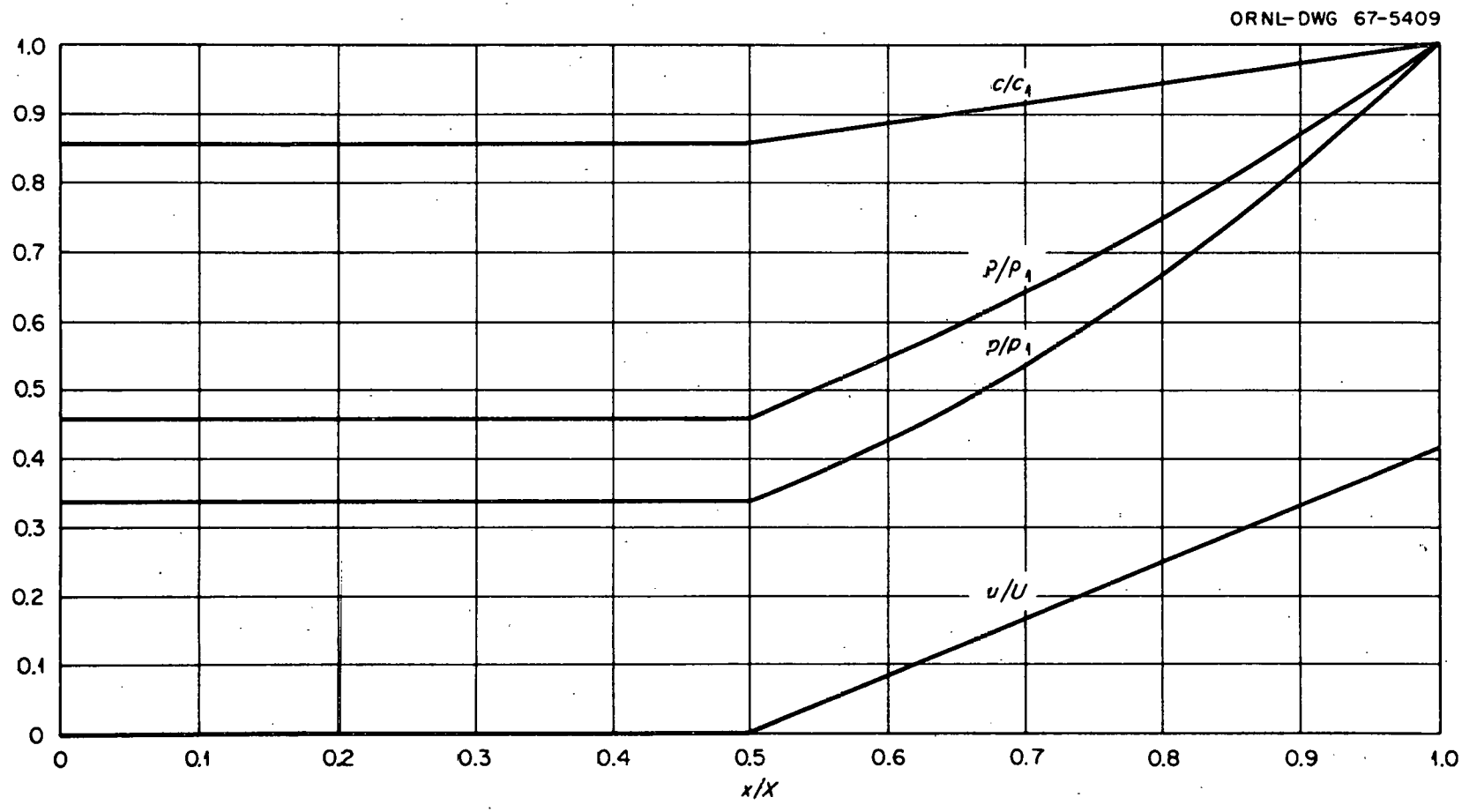

Fig. 7. The Profiles of Flow Velocity, Pressure, Density, and Sonic Velocity Behind the Detonation Front.

5. DISCUSSION

In spite of the complexity of the calculations carried out in sections 3 and 4, they yield only the crudest information about the flow processes occurring in the tube. Much more information can be obtained from the numerical calculations, especially if we examine the pressure, density, and velocity distributions behind the shock front.

Shown in Fig. 8 are seven sets of pressure, density, and velocity distributions corresponding to the seven lettered points in Fig. 2. In these figures, the abscissa $y = X/7.5L$. Thus an abscissa of 0.1333 corresponds to $X = L$, an abscissa of 0.3333 corresponds to $X = 2.500L$, and an abscissa of 0.5089 corresponds to $X = 3.817L$. p_*/p_0 was taken to be 1000 in these calculations. The ordinate labeled "pressure" is $p/2\gamma p_0 = 0.35714\ (p/p_0)$, that labeled "density" is $.50\ (\rho/\rho_0)$, and that labeled "velocity" is $20\ (u/c_0)$.

Figure 8a shows the situation shortly after the rupture of the membrane. The shock front has an abscissa y of approximately 0.160. (In the method of Richtmyer and von Neumann,[3] shocks, which are abrupt discontinuities, are replaced by rapid but continuous changes.) The contact discontinuity is located at about $y = 0.155$. The rarefaction begins at about $y = 0.130$. The region of flow between the shock and the beginning of the rarefaction has a uniform pressure and flow velocity, as it should. The density distribution should consist of two uniform regions separated by the discontinuity at the contact surface. (These regions are somewhat distorted in Fig. 8a because only a small number of mesh points were available at this early stage of the calculation to represent them. They are better developed and more accurately rendered in Fig. 8b.) Behind the rarefaction is the remaining portion of the driver region.

According to the data in Table 1, the pressure just behind the shock should be $0.4609\ p_*$. Thus, the pressure ordinate should be $0.35714 \times 0.4609 \times 1000 = 165$, which is very close to the value shown is Figs. 8a and 8b. (The fluctuations in Fig. 8b are spurious and

result from the finite-difference scheme.) According to the Rankine-Hugoniot equations, a shock with $p_1/p_0 = 460.9$ should have $\rho_1/\rho_0 = 5.925$, which is about 1% less than the value shown in Table 1. This corresponds to an ordinate of about 296 for the density, which is close to the value shown in Fig. 8b. Behind the contact discontinuity, the density ordinate should be 0.5751 x 50 = 28.76 according to Table 1; and this too is in good agreement with the value shown in Fig. 8b. Finally, the ordinate of flow velocity behind the shock front should be 331 [$u_1/c_0 = 16.56$, from Eqs. (12c) and (9a)], which is again close to the value in Figs. 8a and 8b.

In Fig. 8b, the rarefaction has just reached the closed end of the tube. Although region 3 in Fig. 4 has now disappeared, the other regions are still unaffected. In Fig. 8c, the rarefaction has been reflected off the end of the tube and is now advancing into region 2. At this point, X/L is about 2.34, so that conditions at the shock cannot as yet have been affected. In Fig. 8d, X/L = 3.19, and the rarefaction still has not caught up with the shock front. The contact surface is still plainly discernible.

In Fig. 8e, X/L = 4.08, and we are now on the branch (4) of the overpressure curve. The portions of the pressure, density, and flow velocity profiles just behind the shock front are beginning to resemble those behind the shocks originating from a plane explosion when those shocks are strong (Taylor's similarity solution; see Fig. 9). This resemblance increases through Figs. 8f and 8g. For example, in Fig. 8g, at y = 0.69, the pressure, density, and flow velocity are 68%, 55%, and 84% of their respective values at the shock front. The corresponding percentages from Fig. 9 are 69%, 52%, and 86%, respectively.

It appears from these results that in the interval $1 \leq X/L \leq 3.817$ the pressure, density, and velocity profiles just behind the shock front are adjusting their shapes gradually to conform with the shape required by the similarity solution and that while this adjustment is going on, the shock overpressure is unaffected.

Figure 10 shows ten sets of pressure, density, and velocity distributions corresponding to the ten lettered points in Fig. 3. The abscissa in this figure is y = X/4L. p_*/p_0 is now 500, and the ordinate scales are now $p/\gamma p_0 = 0.71428\ (p/p_0)$, $50\ (\rho/\rho_0)$, and $20\ (u/c_0)$.

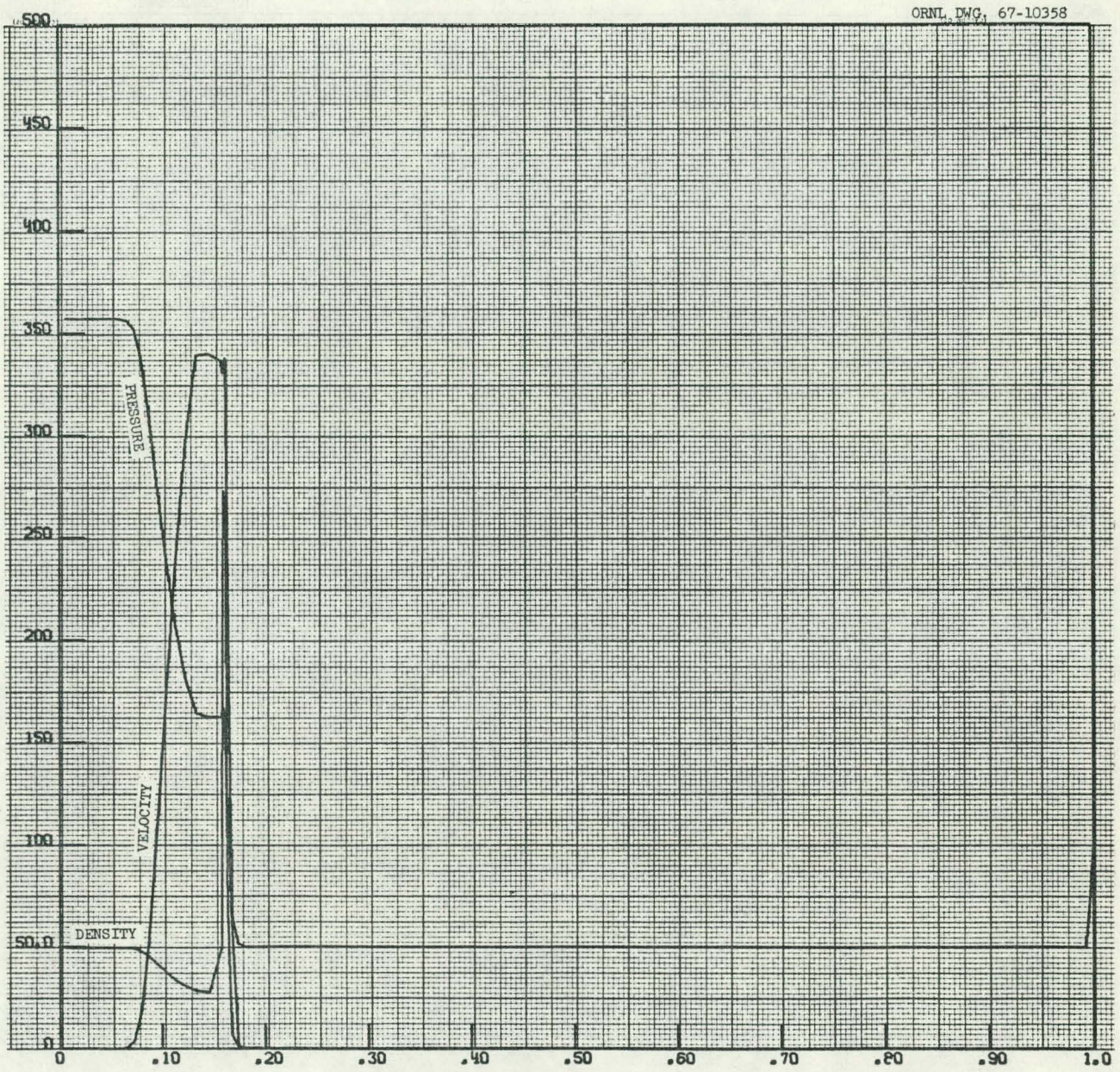

Fig. 8a. The Profiles of Flow Velocity, Pressure, and Density Corresponding to the Lettered Points in Fig. 2.

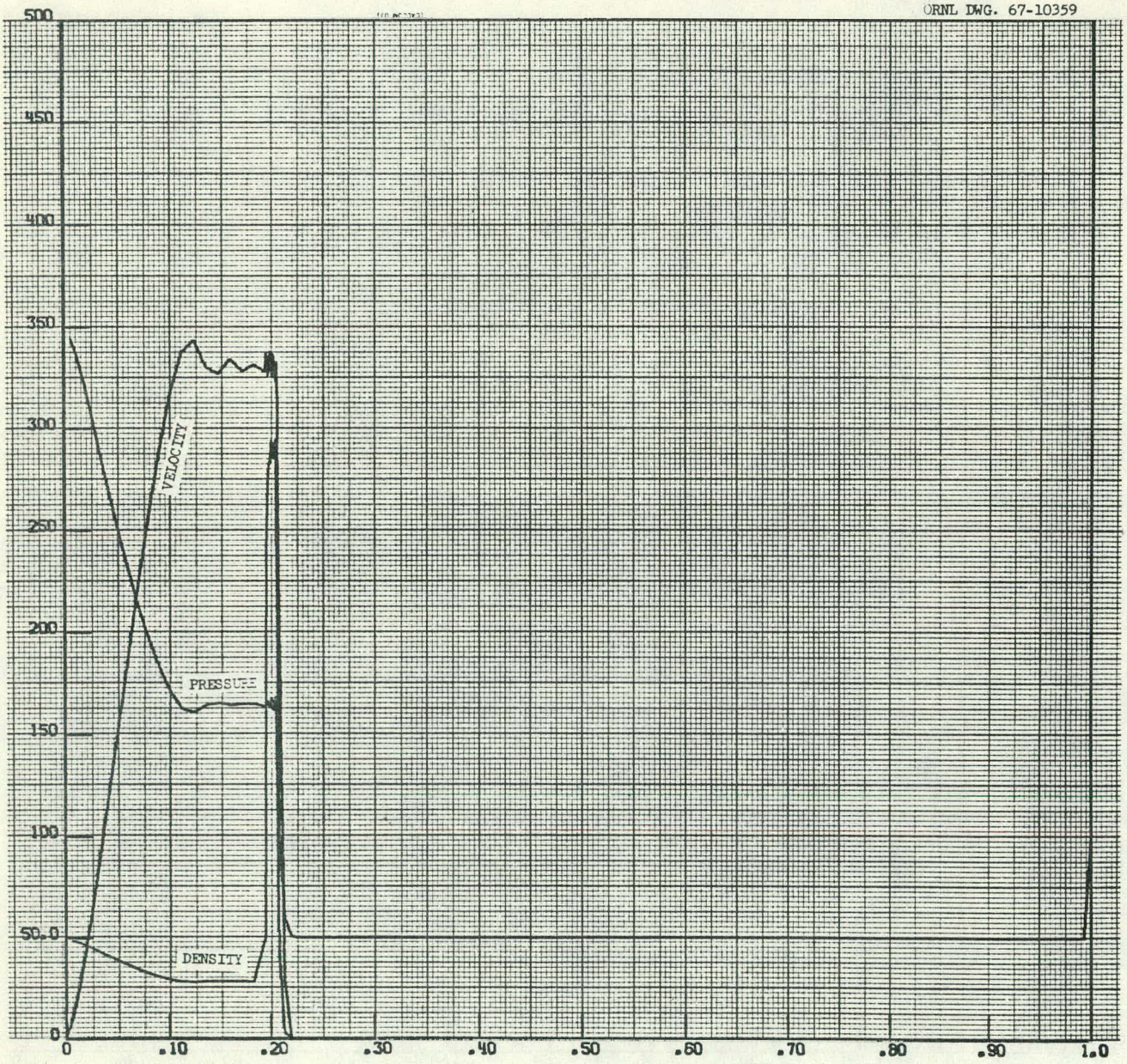

Fig. 8b. The Profiles of Flow Velocity, Pressure, and Density Corresponding to the Lettered Points in Fig. 2.

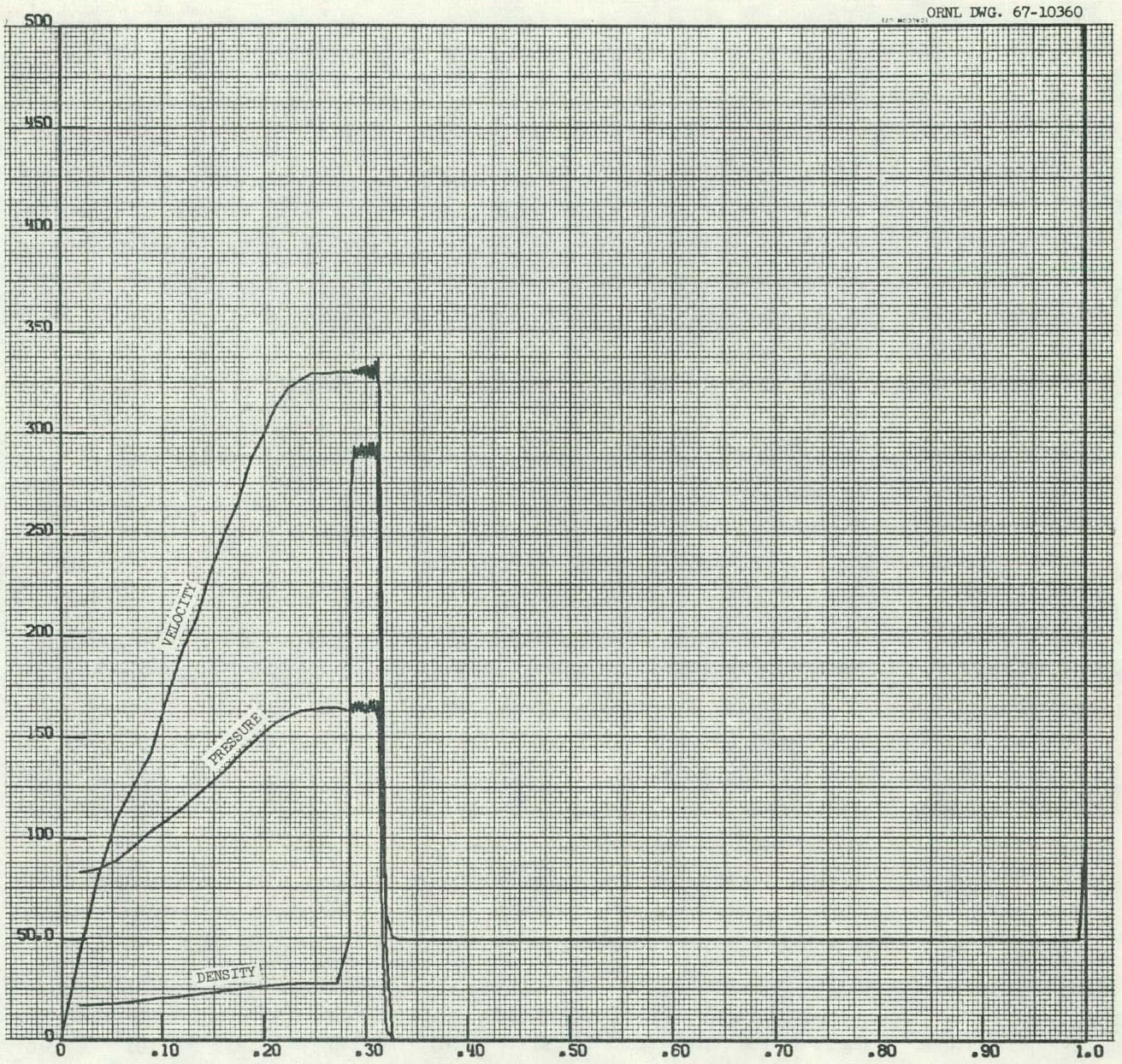

Fig. 8c. The Profiles of Flow Velocity, Pressure, and Density Corresponding to the Lettered Points in Fig. 2.

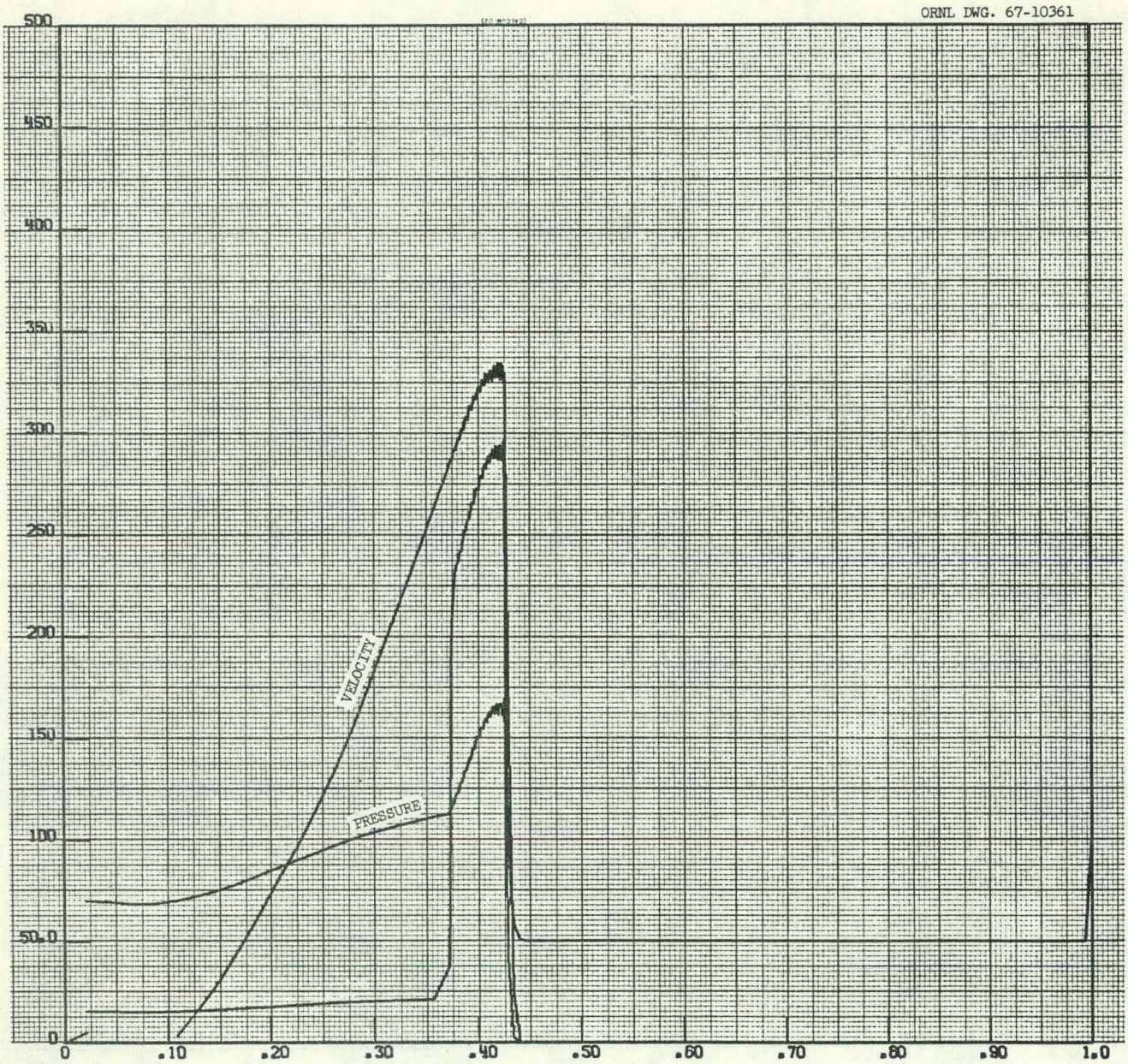

Fig. 8d. The Profiles of Flow Velocity, Pressure, and Density Corresponding to the Lettered Points in Fig. 2.

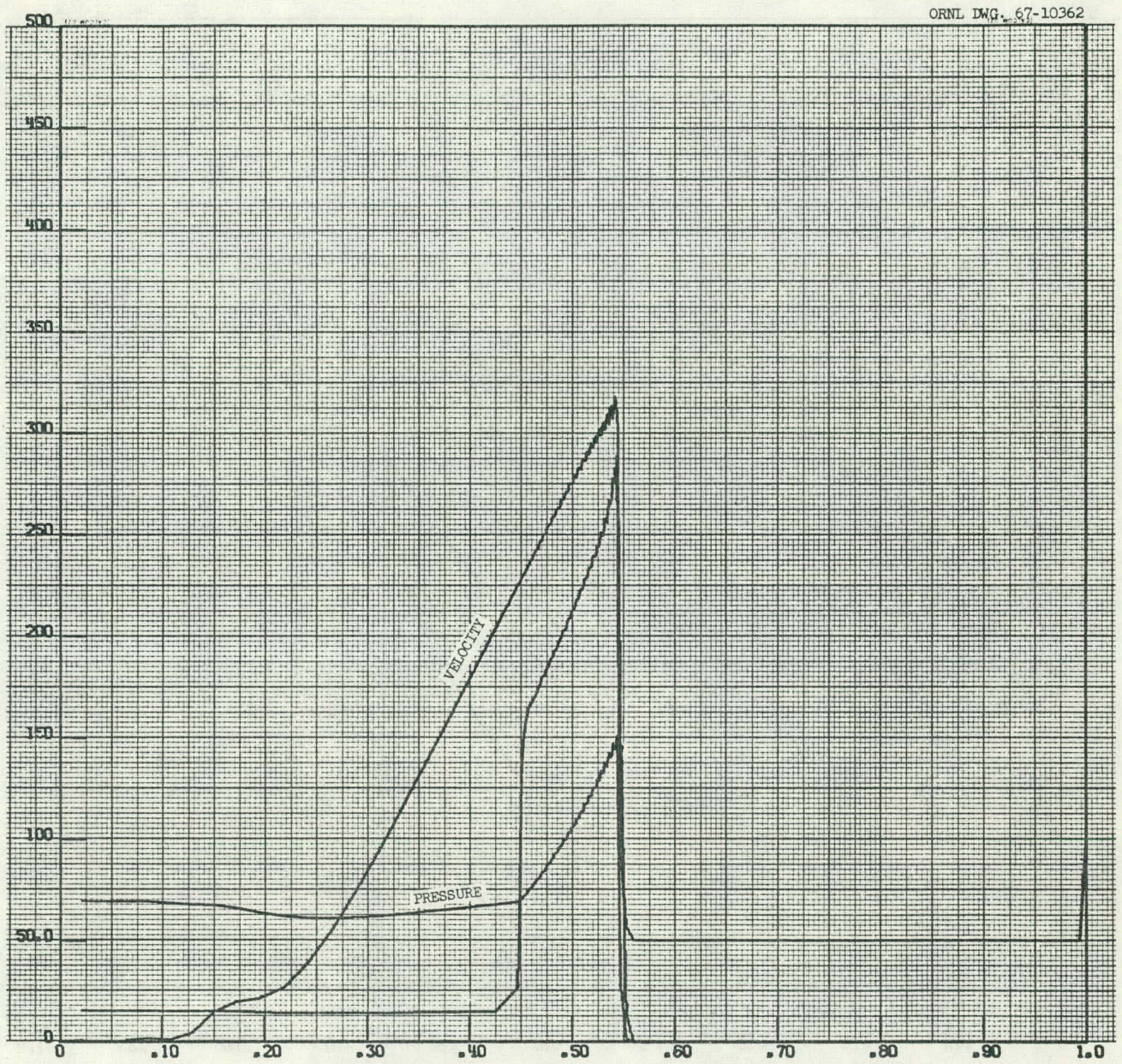

Fig. 8e. The Profiles of Flow Velocity, Pressure, and Density Corresponding to the Lettered Points in Fig. 2.

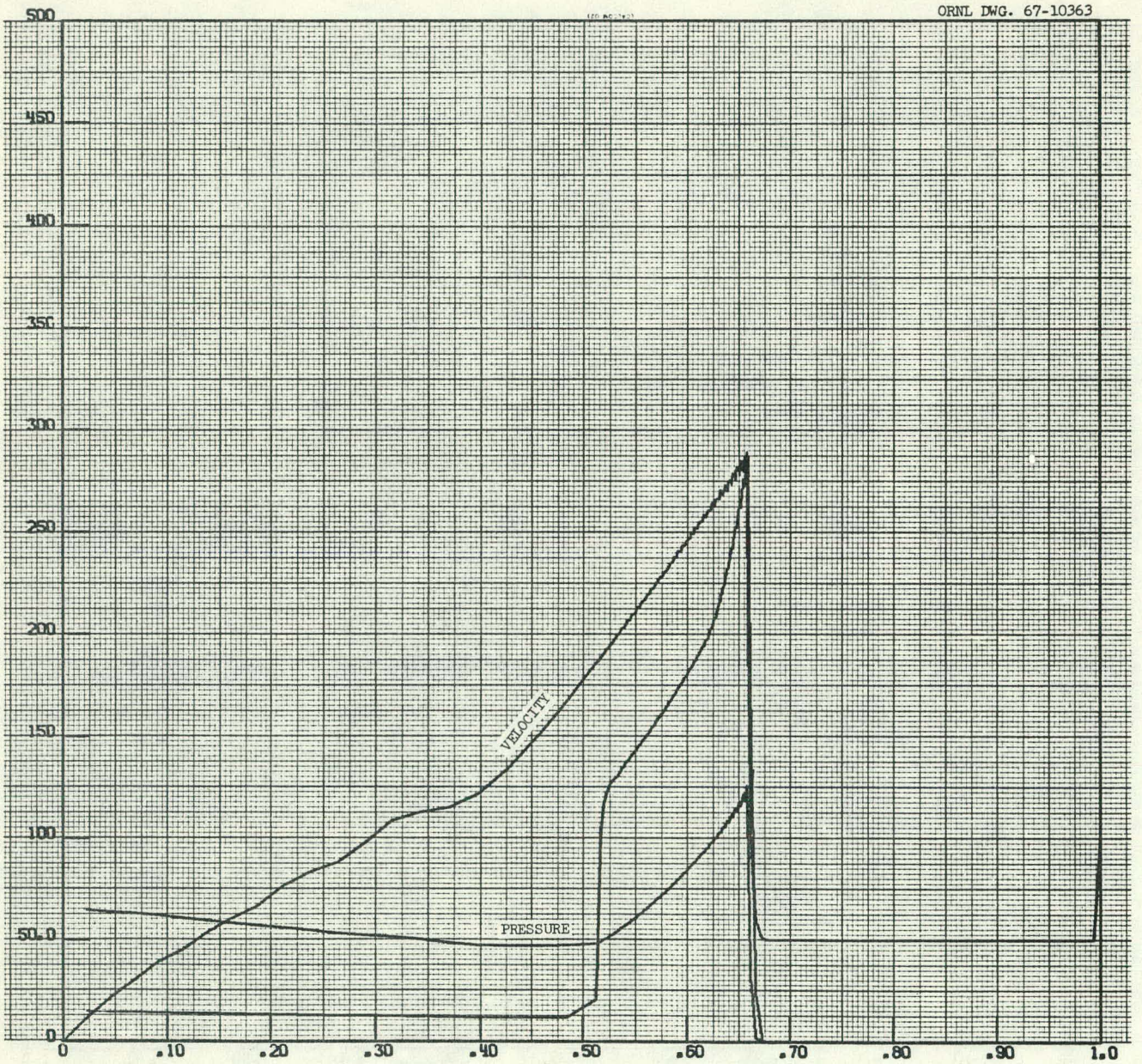

Fig. 8f. The Profiles of Flow Velocity, Pressure, and Density Corresponding to the Lettered Points in Fig. 2.

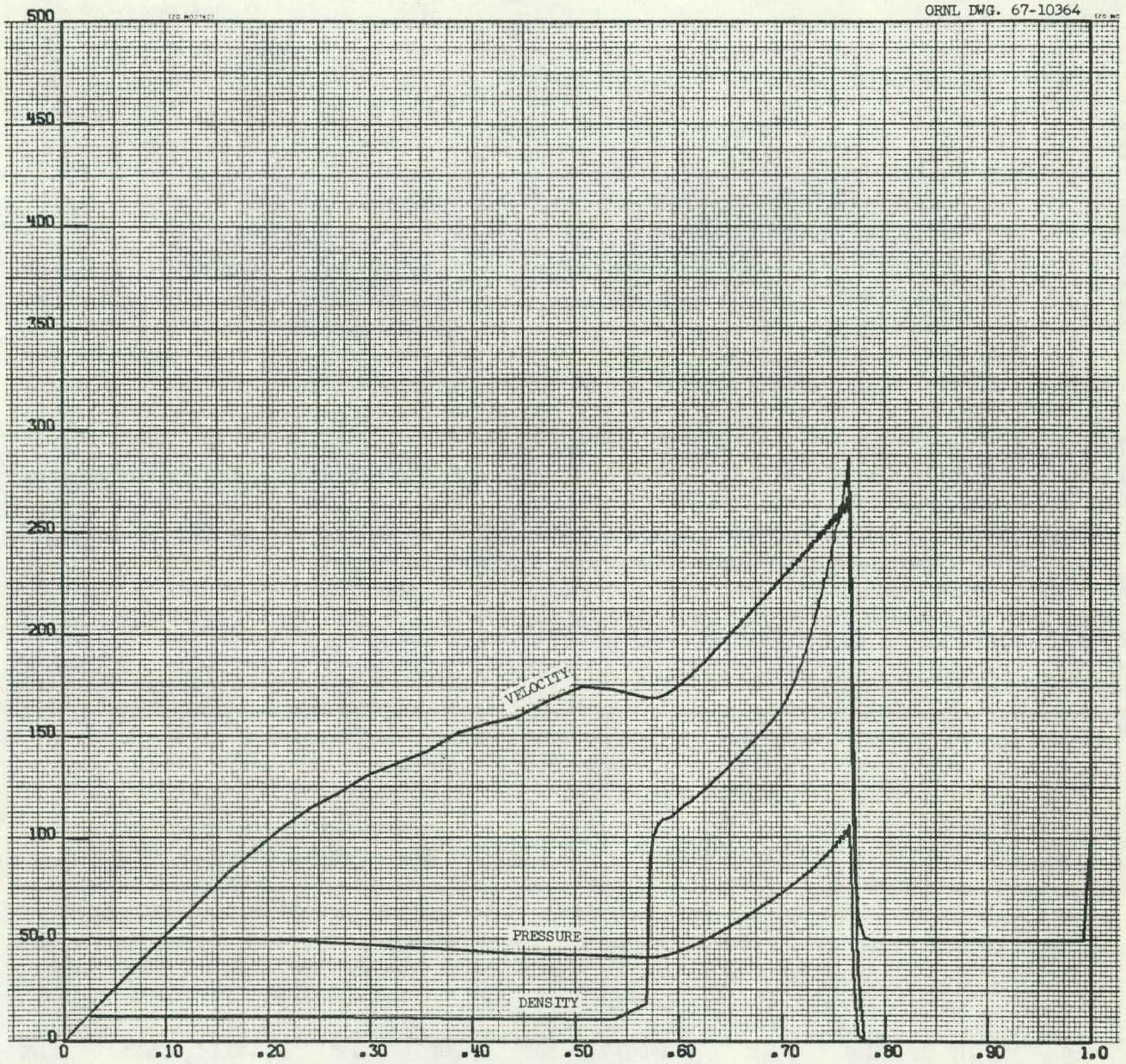

Fig. 8g. The Profiles of Flow Velocity, Pressure, and Density Corresponding to the Lettered Points in Fig. 2.

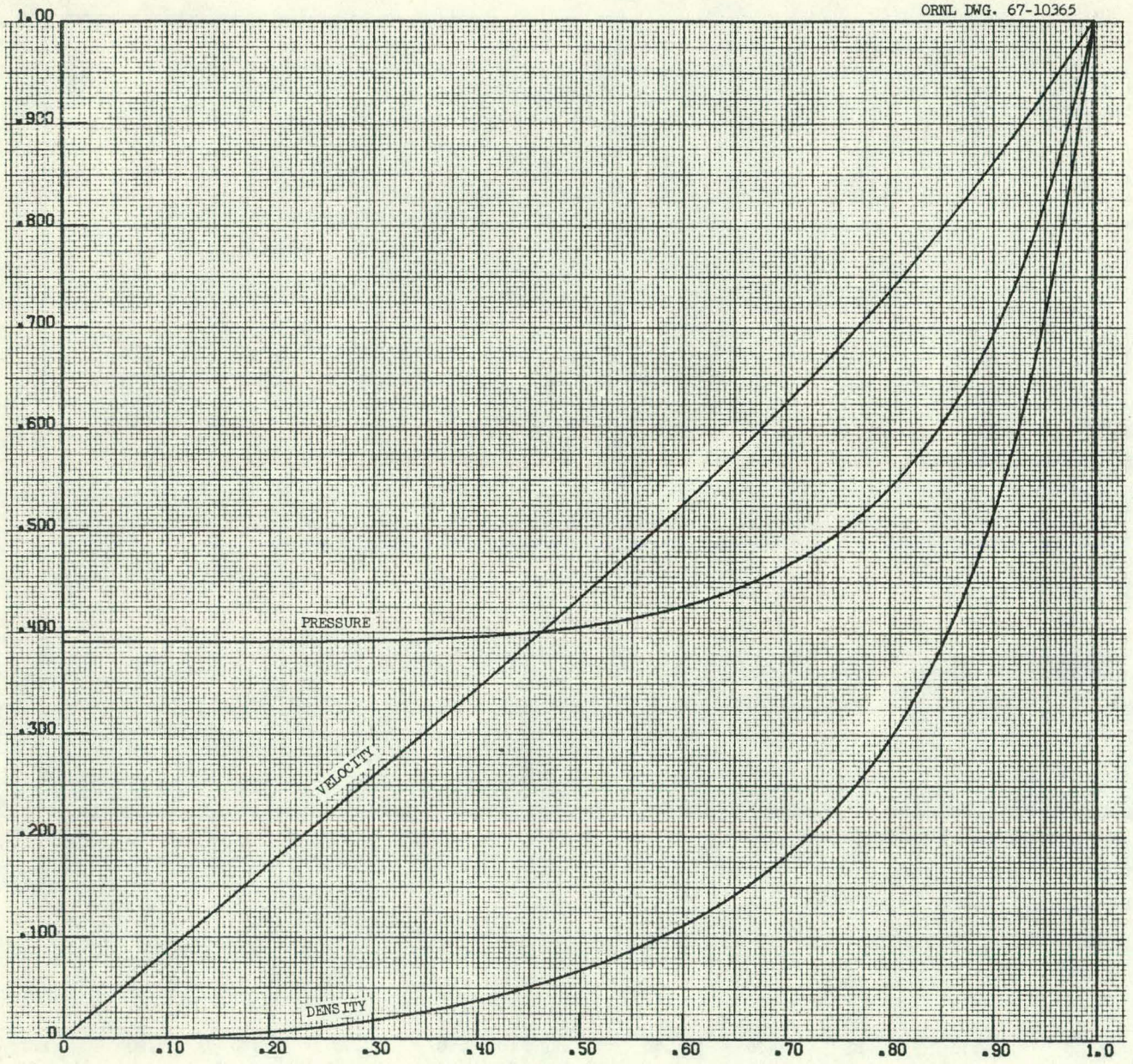

Fig. 9. The Profiles of Flow Velocity, Pressure, and Density for the Similarity Solution of Taylor, von Neumann, and Sedov.

Figure 10a shows the situation shortly after the detonation front passes the point X = L. Behind a value of y of about 0.23, the initial pressure, density, and flow velocity distributions (shown in Fig. 7) are as yet undisturbed. In front of y = 0.23, a rarefaction, a contact discontinuity, and a shock front have formed. By the time X/L has reached 1.9 (Fig. 10d), the shock pressure has fallen below the pressure of the gas in region 2 of Fig. 5. This gas can now expand forward and even strengthen the shock. This expansion is shown in Figs. 10e-j. By the time X/L has reached 3.0 (Fig. 10g), the gas expanding forward has begun to support the shock front. In Figs. 10h-j this support is evidenced by the constancy of the shock strength. However, the profiles of pressure, density and flow velocity are changing from concave downwards to concave upwards and approaching the profiles of the similarity solution. The region of constant shock overpressure between 3.3L and 5.0L in this problem is the analogue of the region of constant overpressure between L and 3.817L in the case of uniform heating. Beyond 5.0L the overpressure follows branch (7) of the overpressure curve quite closely.

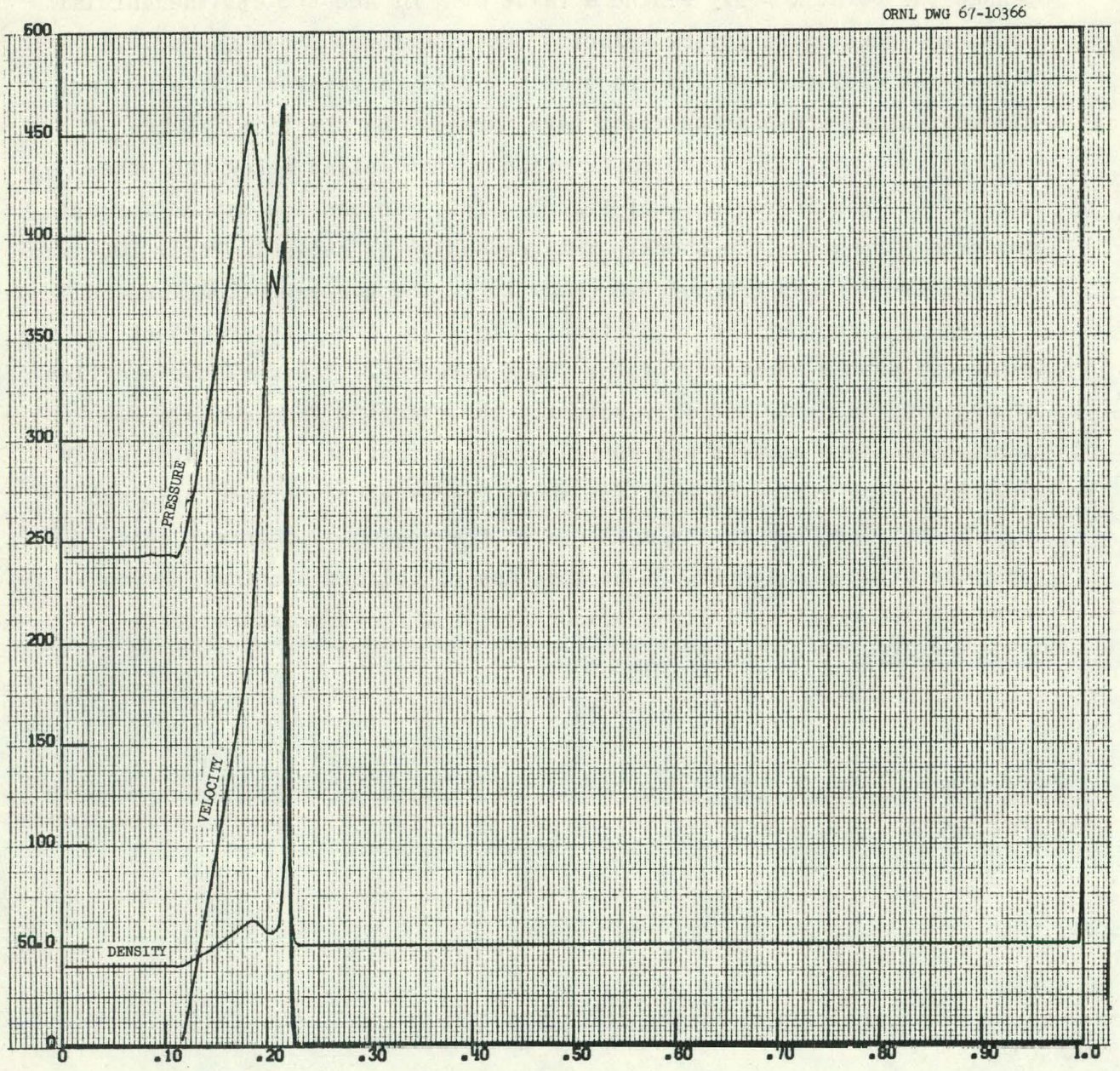

Fig. 10a. The Profiles of Flow Velocity, Pressure, and Density Corresponding to the Lettered Points in Fig. 3.

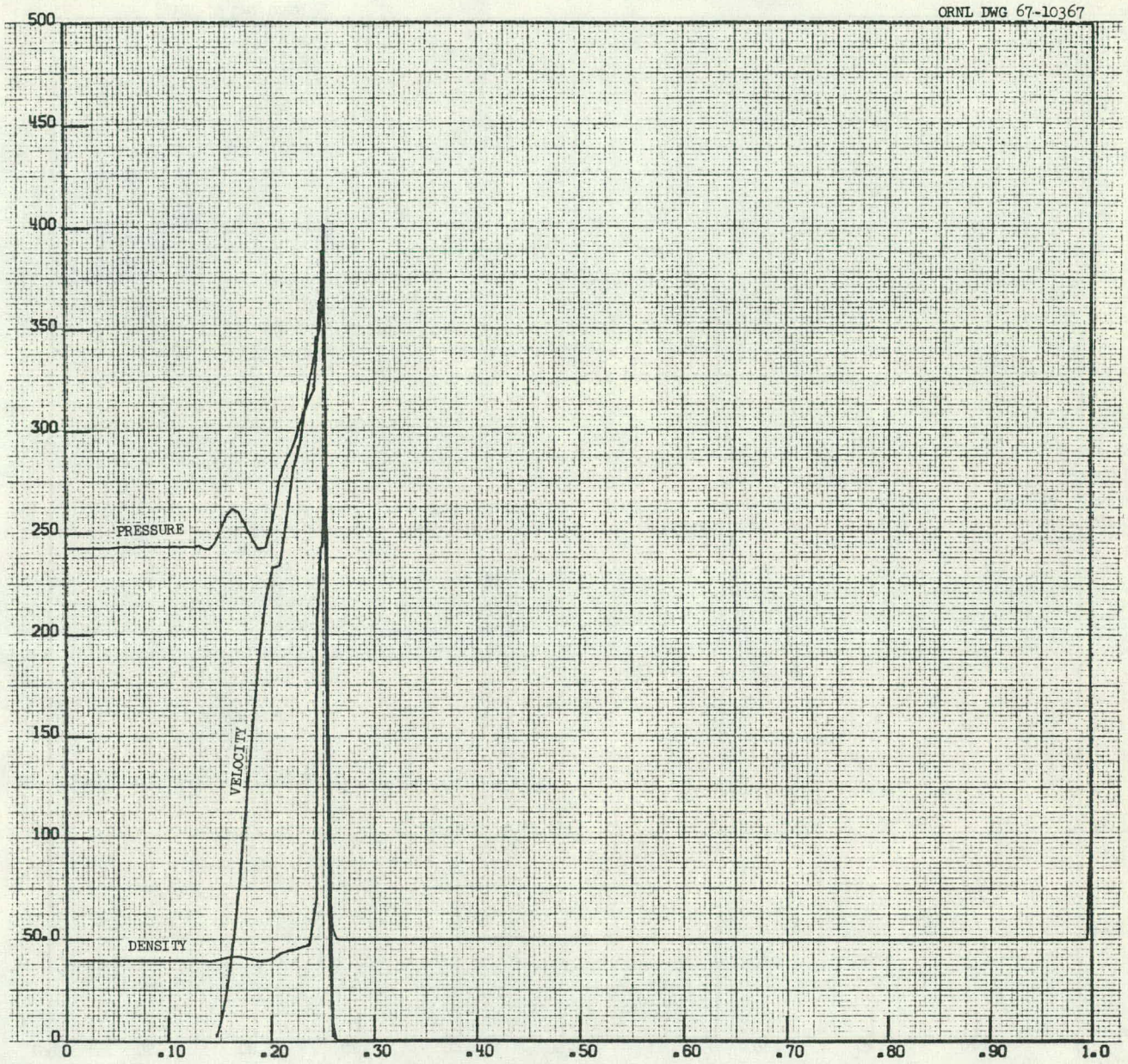

Fig. 10b. The Profiles of Flow Velocity, Pressure, and Density Corresponding to the Lettered Points in Fig. 3.

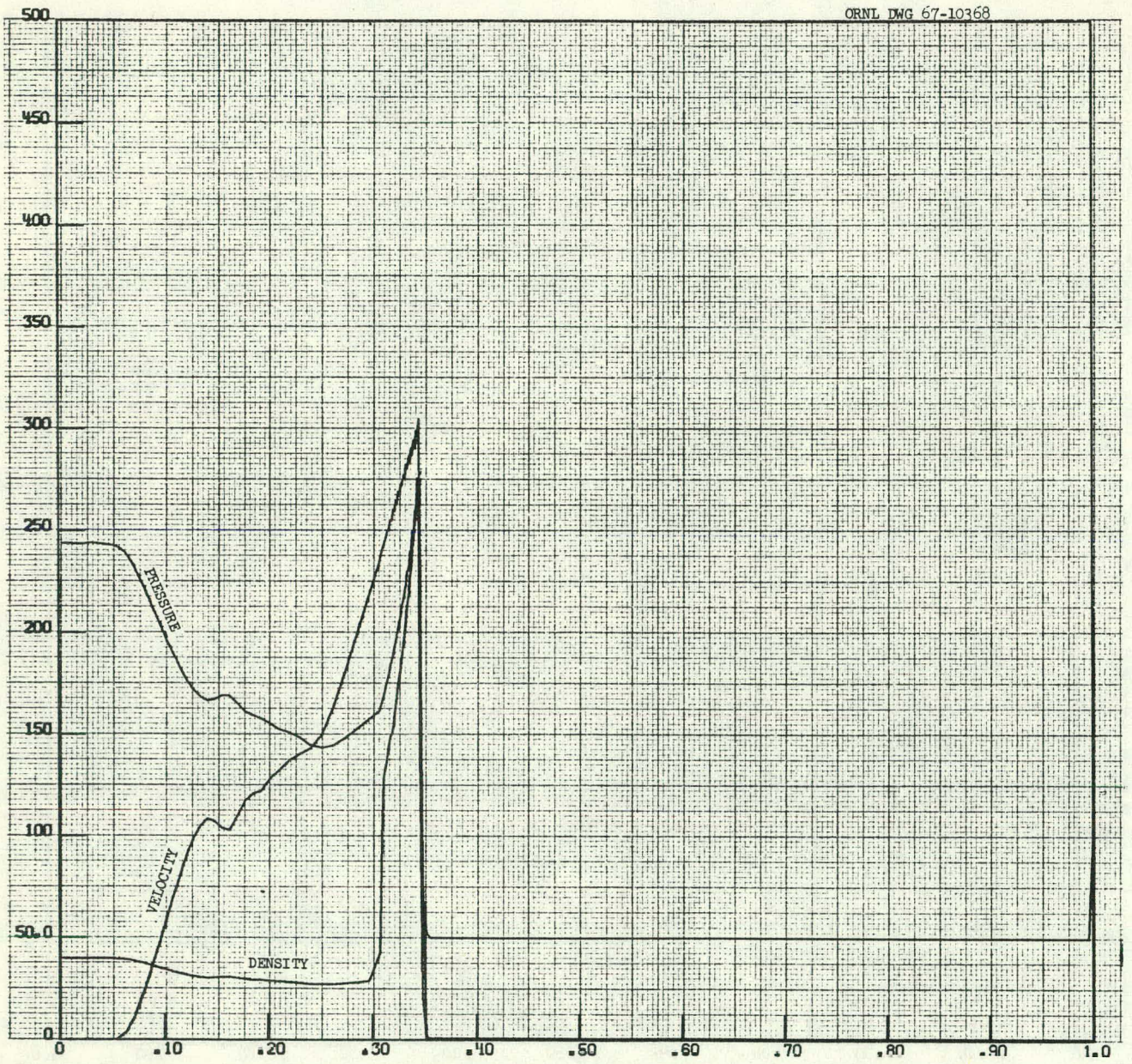

Fig. 10c. The Profiles of Flow Velocity, Pressure, and Density Corresponding to the Lettered Points in Fig. 3.

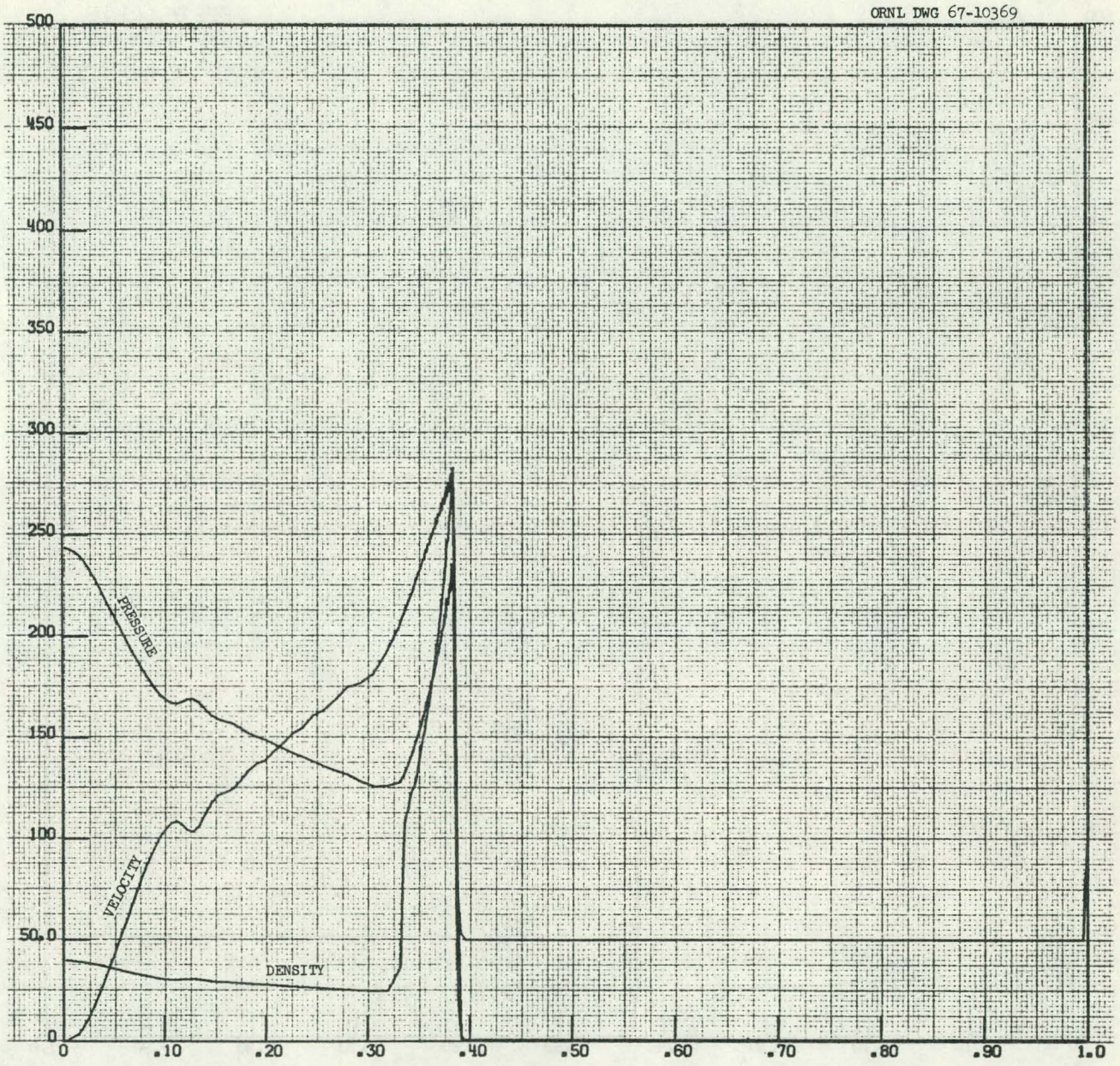

Fig. 10d. The Profiles of Flow Velocity, Pressure, and Density Corresponding to the Lettered Points in Fig. 3.

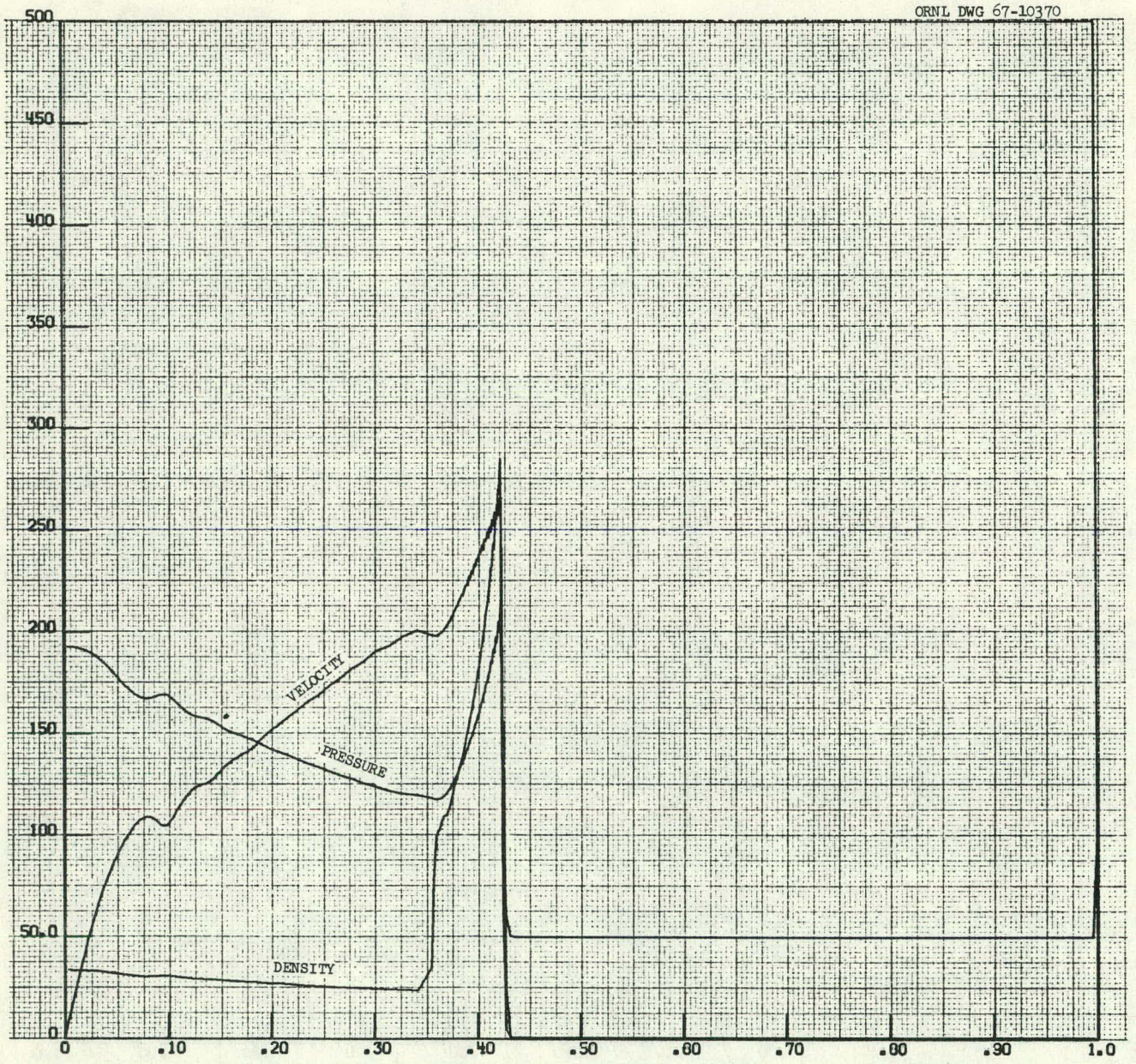

Fig. 10e. The Profiles of Flow Velocity, Pressure, and Density Corresponding to the Lettered Points in Fig. 3.

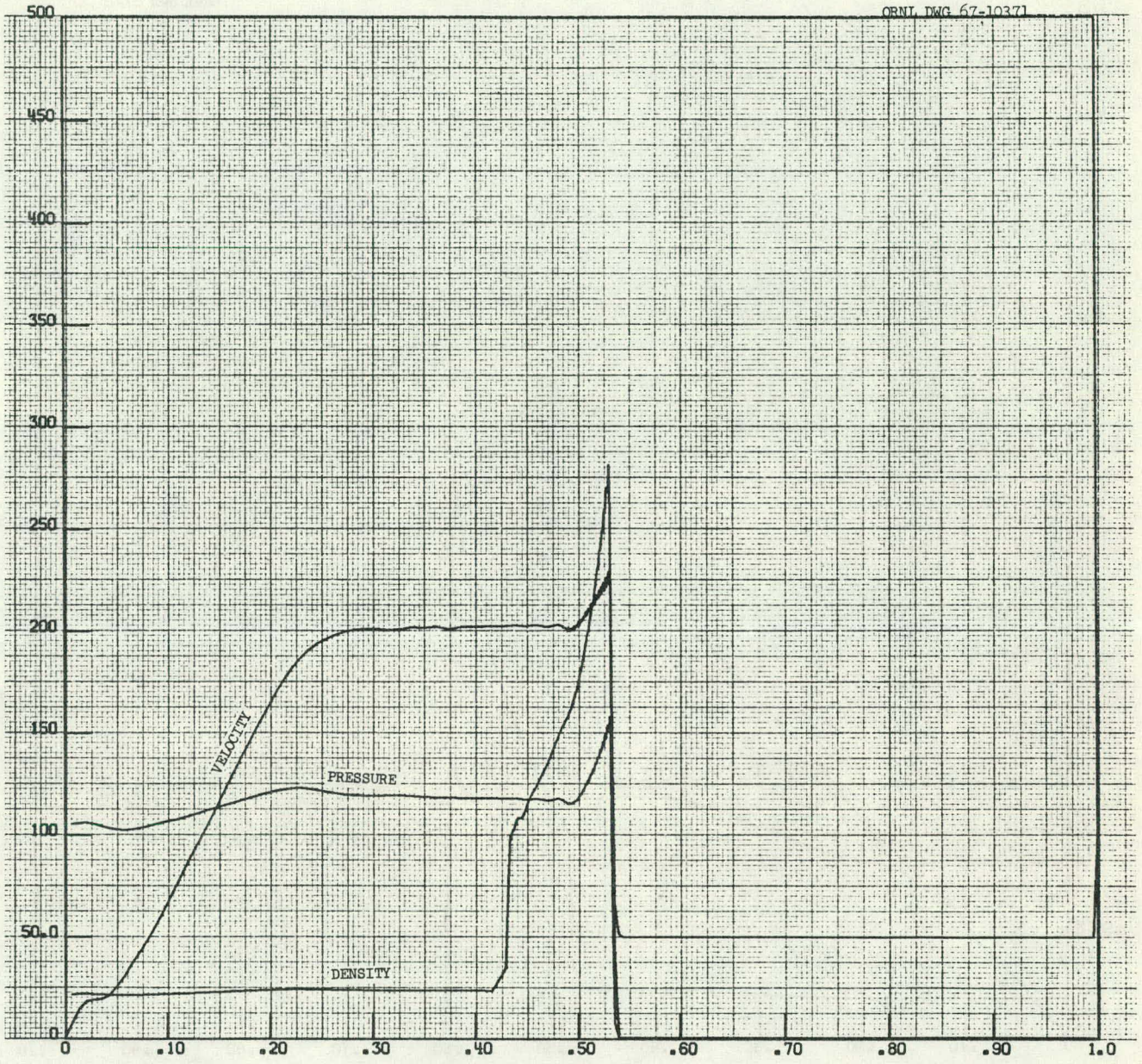

Fig. 10f. The Profiles of Flow Velocity, Pressure, and Density Corresponding to the Lettered Points in Fig. 3.

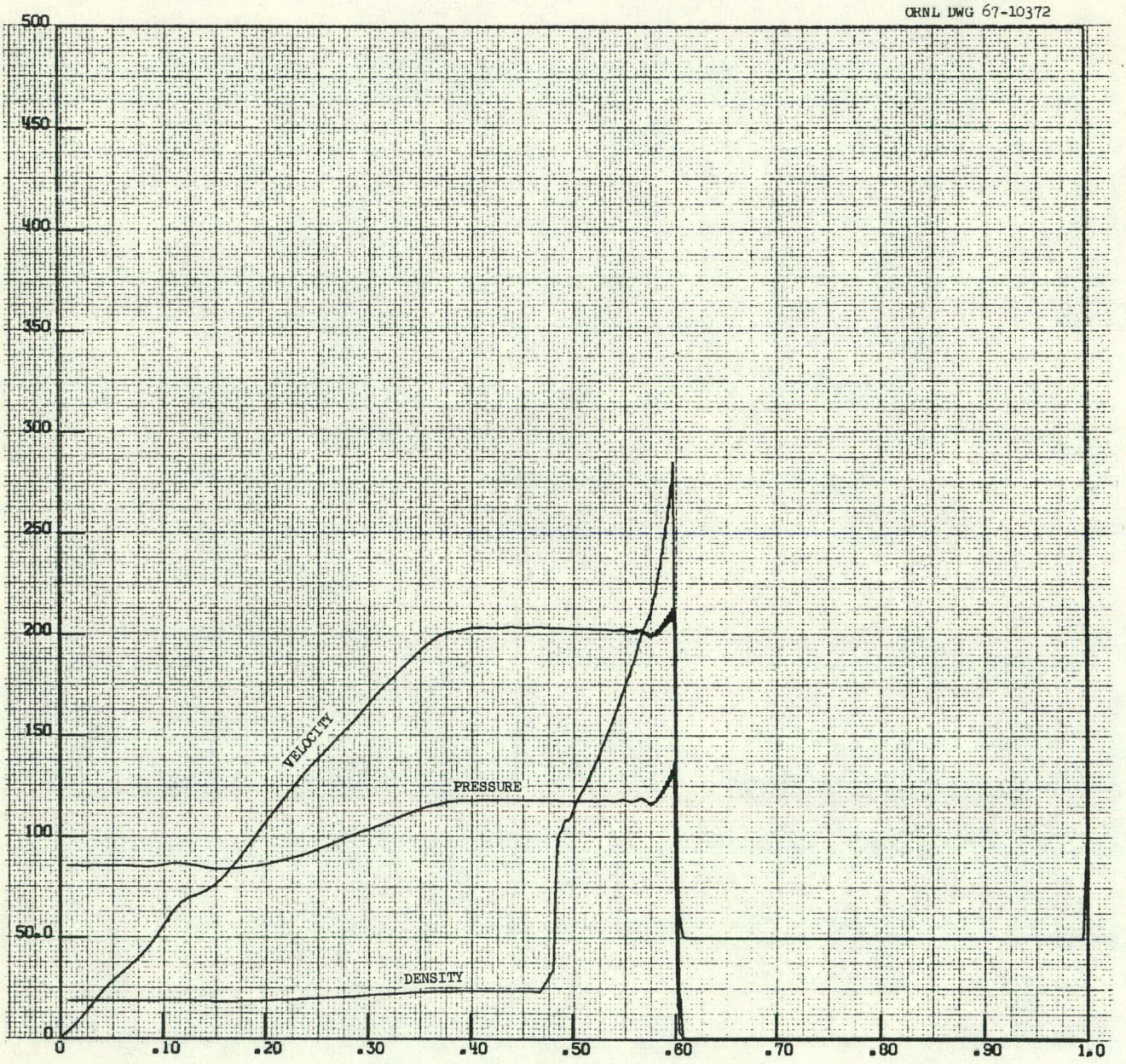

Fig. 10g. The Profiles of Flow Velocity, Pressure, and Density Corresponding to the Lettered Points in Fig. 3.

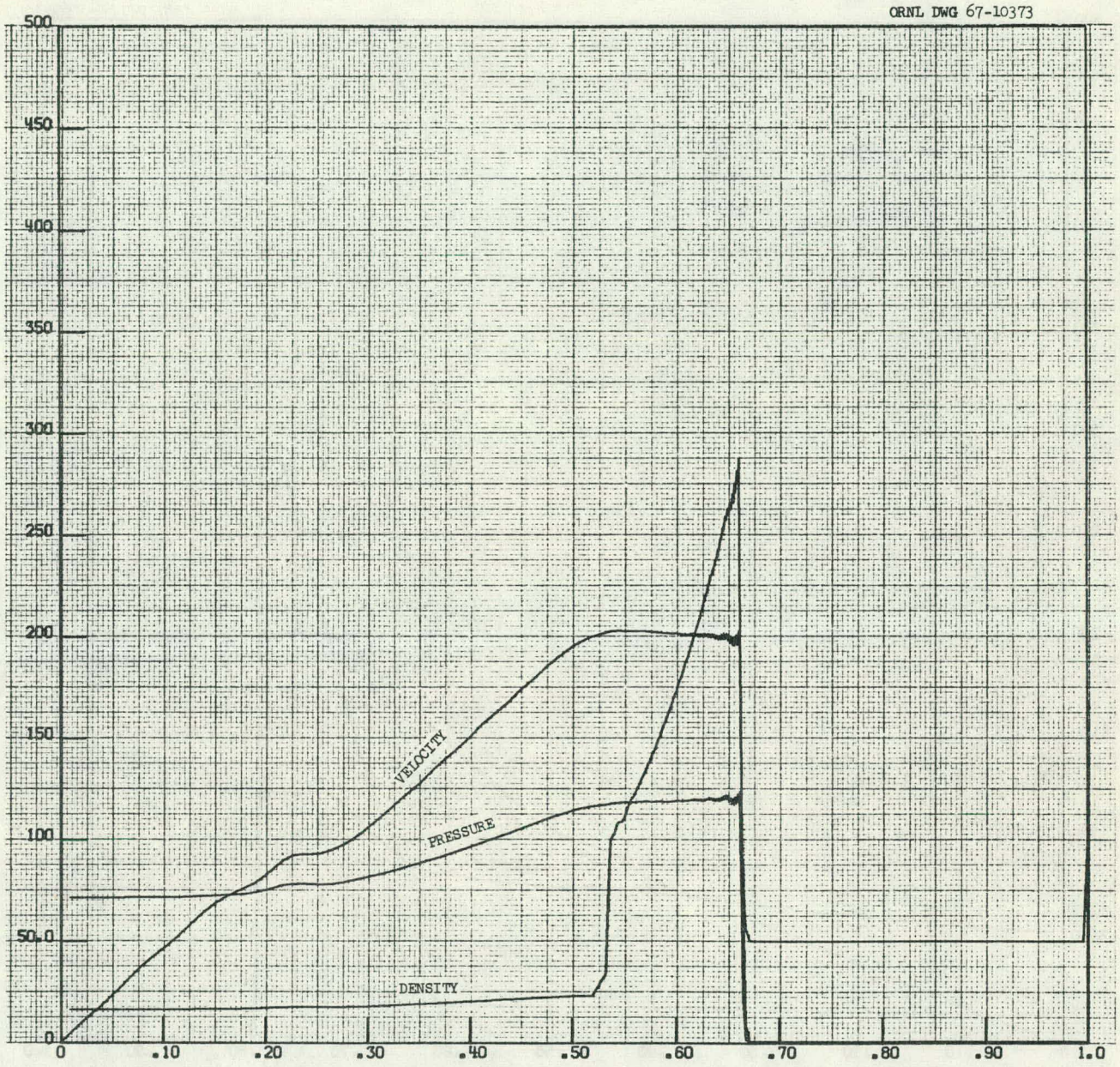

Fig. 10h. The Profiles of Flow Velocity, Pressure, and Density Corresponding to the Lettered Points in Fig. 3.

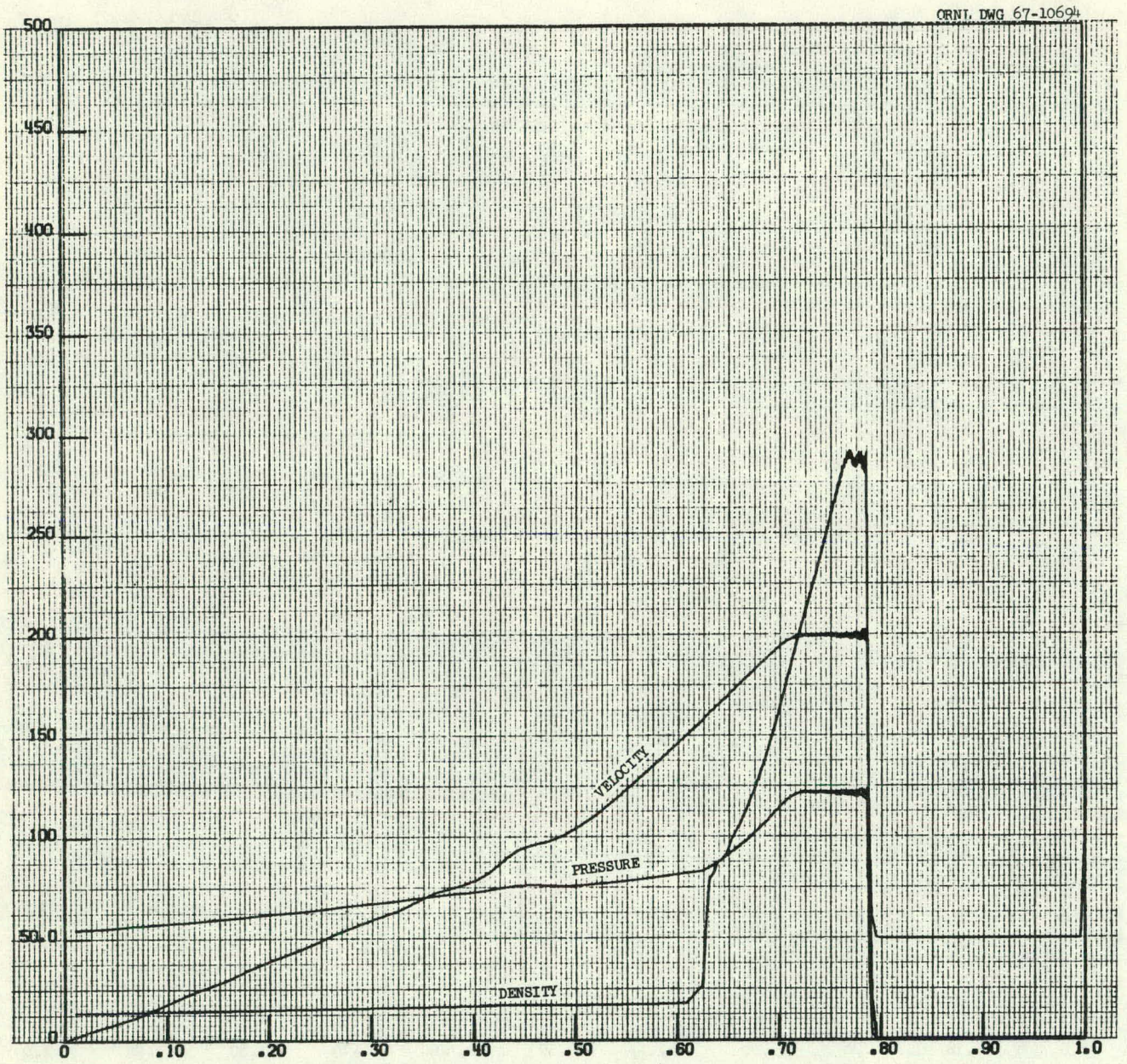

Fig. 10i. The Profiles of Flow Velocity, Pressure, and Density Corresponding to the Lettered Points in Fig. 3.

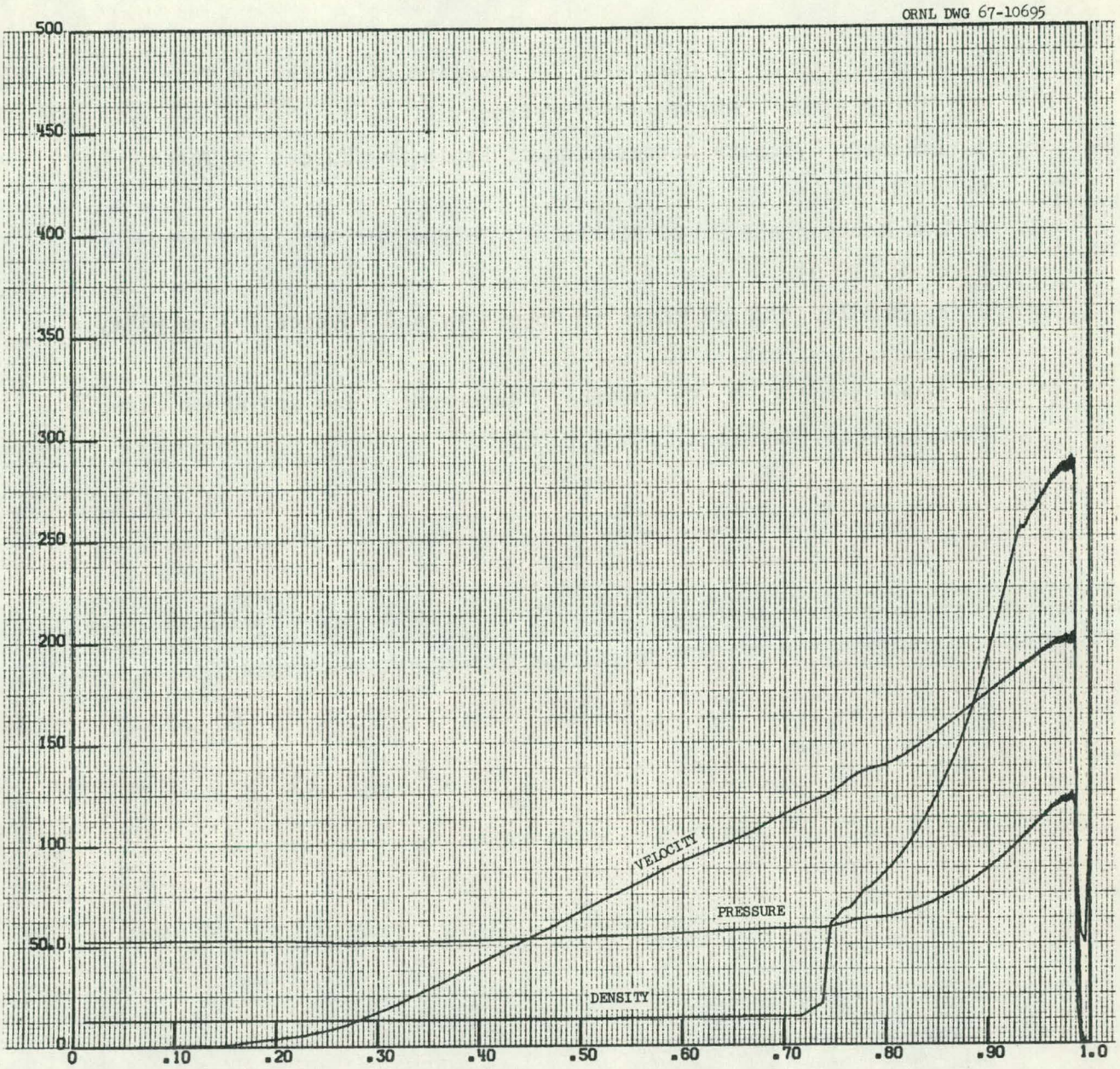

Fig. 10j. The Profiles of Flow Velocity, Pressure, and Density Corresponding to the Lettered Points in Fig. 3.

REFERENCES

1. L. Dresner and C. V. Chester, "Attenuation of Shocks in Tubes by Orifice Plates," ORNL-TM-1750, February 9, 1967.
2. L. Dresner, "Viscous Attenuation of Explosive Shocks in Tubes," ORNL-TM-1823.
3. J. von Neumann and R. D. Richtmyer, Journal of Applied Physics 21 232 (1950).
4. J. N. Bradley, "Shock Waves in Chemistry and Physics," John Wiley and Sons, New York, 1962, p. 48.
5. R. Courant and K. O. Friedrichs, "Supersonic Flow and Shock Waves," Interscience, New York, 1948, p. 223.

ORNL-TM-1966

INTERNAL DISTRIBUTION

1. J. C. Bresee
2-11. C. V. Chester
12-21. L. Dresner
22. C. M. Haaland
23. J. L. Liverman
24. F. C. Maienschein
25. R. A. Uher
26. A. M. Weinberg
27. E. P. Wigner
28-42. Civil Defense Project Library
43-44. Central Research Library
45. ORNL-Y-12 Technical Library, Document Reference Section
46-48. Laboratory Records Department
49. Laboratory Records, ORNL RC
50. ORNL Patent Office
51. Laboratory and University Div. ORO
52-66. Division of Technical Information Extension

EXTERNAL DISTRIBUTION

67. Harold M. Agnew, Weapons Physics Division, Los Alamos Scientific Laboratory, Los Alamos, New Mexico
68. William Brown, Hudson Institute, Harmon-on-Hudson, New York
69-79. L. J. Deal, Civil Effects Branch, Division of Biology and Medicine, U. S. Atomic Energy Commission, Washington, D. C.
80. Grace Kelleher, Institute for Defense Analyses, Arlington, Virginia
81. Jack Kelso, Defense Atomic Support Agency, Department of Defense, Washington, D. C.
82. N. E. Landdeck, Office of Civil Defense, Washington, D. C.
83. D. L. Lehto, U. S. Naval Ordnance Laboratory, White Oak, Silver Spring, Maryland
84. Billy McCormac, IITRI, 10 West 35th Street, Chicago, Illinois
85. Clarence Mehl, Sandia Corporation, Albuquerque, New Mexico
86. E. E. Minor, Ballistic Research Laboratory, Aberdeen, New Mexico
87. D. L. Narver, Jr., Holmes and Narver, Inc., 828 S. Figueroa St., Los Angeles, California
88. J. S. Newman, Department of Chemical Engineering, University of California, Berkeley, California
89. Edgar Parsons, Research Triangle Institute, Raleigh, North Carolina
90. L. Rudlin, U. S. Naval Ordnance Laboratory, White Oak, Silver Spring, Maryland
91. M. Rubenstein, Defense Atomic Support Agency, Department of Defense, Washington, D. C.
92. Col. Ralph Pennington, Advanced Research Projects Agency, Department of Defense, Washington, D. C.
93. Duane Sewell, Lawrence Radiation Laboratory, Livermore, California
94-103. W. E. Strope, Office of Civil Defense, Washington, D. C.
104. William Taylor, Ballistic Research Laboratory, Aberdeen, Maryland
105. William A. Whitaker, Air Force Weapons Laboratory, Kirtland Air Force Base, Albuquerque, New Mexico
106. William White, Stanford Research Institute, Stanford, California
107. Paul Zigmun, U. S. Naval Radiological Defense Laboratory, Hunter's Point, San Francisco, California